



Chemical aging of single and multicomponent biomass burning aerosol surrogate particles by OH: implications for cloud condensation nucleus activity

J. H. Slade¹, R. Thalman², J. Wang², and D. A. Knopf¹

¹Institute for Terrestrial and Planetary Atmospheres, School of Marine and Atmospheric Sciences, State University of New York at Stony Brook, Stony Brook, NY 11794, USA

²Brookhaven National Laboratory, Department of Environmental and Climate Sciences, Upton, NY 11973, USA

Correspondence to: D. A. Knopf (daniel.knopf@stonybrook.edu)

Received: 11 February 2015 – Published in Atmos. Chem. Phys. Discuss.: 6 March 2015

Revised: 15 August 2015 – Accepted: 1 September 2015 – Published: 14 September 2015

Abstract. Multiphase OH and O₃ oxidation reactions with atmospheric organic aerosol (OA) can influence particle physicochemical properties including composition, morphology, and lifetime. Chemical aging of initially insoluble or low-soluble single-component OA by OH and O₃ can increase their water solubility and hygroscopicity, making them more active as cloud condensation nuclei (CCN) and susceptible to wet deposition. However, an outstanding problem is whether the effects of chemical aging on their CCN activity are preserved when mixed with other organic or inorganic compounds exhibiting greater water solubility. In this work, the CCN activity of laboratory-generated biomass burning aerosol (BBA) surrogate particles exposed to OH and O₃ is evaluated by determining the hygroscopicity parameter, κ , as a function of particle type, mixing state, and OH and O₃ exposure applying a CCN counter (CCNc) coupled to an aerosol flow reactor (AFR). Levoglucosan (LEV), 4-methyl-5-nitrocatechol (MNC), and potassium sulfate (KS) serve as representative BBA compounds that exhibit different hygroscopicity, water solubility, chemical functionalities, and reactivity with OH radicals, and thus exemplify the complexity of mixed inorganic/organic aerosol in the atmosphere. The CCN activities of all of the particles were unaffected by O₃ exposure. Following exposure to OH, κ of MNC was enhanced by an order of magnitude, from 0.009 to ~ 0.1 , indicating that chemically aged MNC particles are better CCN and more prone to wet deposition than pure MNC particles. No significant enhancement in κ was

observed for pure LEV particles following OH exposure. κ of the internally mixed particles was not affected by OH oxidation. Furthermore, the CCN activity of OH-exposed MNC-coated KS particles is similar to the OH unexposed atomized 1 : 1 by mass MNC : KS binary-component particles. Our results strongly suggest that when OA is dominated by water-soluble organic carbon (WSOC) or inorganic ions, chemical aging has no significant impact on OA hygroscopicity. The organic compounds exhibiting low solubility behave as if they are infinitely soluble when mixed with a sufficient number of water-soluble compounds. At and beyond this point, the particles' CCN activity is governed entirely by the water-soluble fraction and is not influenced by the oxidized organic fraction. Our results have important implications for heterogeneous oxidation and its impact on cloud formation given that atmospheric aerosol is a complex mixture of organic and inorganic compounds exhibiting a wide range of solubilities.

1 Introduction

The extent to which aerosol–cloud interactions impact the atmospheric radiative budget and climate change is significant, but remains highly uncertain (Stocker et al., 2013). Attributed to this uncertainty is the difficulty in quantifying the effects of chemical aging during atmospheric particle transport by heterogeneous or multiphase chemical reactions between organic aerosol particles and trace gas-phase oxi-

dants and radicals (Abbatt et al., 2012; Pöschl, 2011; George and Abbatt, 2010; Rudich et al., 2007). Heterogeneous oxidation reactions between organic aerosol particles and OH, O₃, or NO₃ can impact the particles' physical and chemical properties (Ellison et al., 1999; Rudich, 2003; Pöschl, 2005; Rudich et al., 2007; George and Abbatt, 2010), and have been shown to impact particle hygroscopicity and cloud condensation nuclei (CCN) activity (Broekhuizen et al., 2004; Petters et al., 2006; Shilling et al., 2007; Pöschl, 2011; George et al., 2009) and ice nucleation (IN) (Wang and Knopf, 2011; Brooks et al., 2014).

Cloud nucleation efficiency depends on the particle's water solubility, hygroscopicity, size, and morphology (Petters and Kreidenweis, 2007, 2008; Dusek et al., 2006; Giordano et al., 2015). The majority of submicron aerosol particles are comprised of organic material (Zhang et al., 2007; Hallquist et al., 2009), which possess a wide range of hygroscopicity ($\kappa \sim 0.01\text{--}0.5$) (Petters and Kreidenweis, 2007). A significant portion of atmospheric organic aerosol (OA) is derived from biomass burning (BB) emissions (Bond et al., 2004; Andreae et al., 2004; Hays et al., 2005; Monks et al., 2009). BB plays an important role both regionally and globally (Park et al., 2007), accounting for an estimated 2.5 Pg C yr^{-1} (van der Werf et al., 2006). Reflectance data from satellite retrievals indicate that BB accounts for a global footprint of 464 Mha yr^{-1} or roughly $\sim 36\%$ of cropland on earth (Randerson et al., 2012). Biomass burning aerosol (BBA) constitutes a significant fraction of primary organic aerosol (POA) (Bond et al., 2004) and secondary organic aerosol (SOA), derived from oxidative aging of volatile and semi-volatile organic vapors emitted from biomass burning plumes (Carrico et al., 2010; Hallquist et al., 2009; Jathar et al., 2014). Molecular markers of BB POA include pyrolyzed forms of glucose such as levoglucosan (LEV, 1-6-anhydro- β -glucopyranose) (Simoneit, 1999) and potassium-containing salts such as potassium sulfate (KS, K₂SO₄) (Sheffield et al., 1994). The photo-oxidation of *m*-cresol, which is emitted at high levels from biomass burning (Schauer et al., 2001), in the presence of NO_x, generates 4-methyl-5-nitrocatechol (MNC), which has recently been recognized as a potentially important tracer for biomass burning SOA (Iinuma et al., 2010). With the exception of MNC, the CCN activity and hygroscopicity of LEV and KS, among other select BBA compounds and smoke particles, have been determined (Petters et al., 2009; Carrico et al., 2010). Dusek et al. (2011) derived κ values of 0.2 for the water-soluble organic content (WSOC) in particles produced from controlled laboratory burns. Carrico et al. (2010) determined a mean κ of 0.1 for carbonaceous particles sampled from open combustion of several biomass fuels. Hygroscopic growth factors of LEV and other biomass burning derived organics range from 1.27 to 1.29 at relative humidity RH = 90% (Chan et al., 2005; Mikhailov et al., 2009). In situ field measurements of the CCN efficiency (ratio of CCN to the available condensation nuclei, CN) of biomass burning smoke particles is on the or-

der of 50% at 1% supersaturation (Andreae et al., 2004). While inorganic ions have only a minor importance as an atmospheric tracer for biomass burning, they can significantly influence the CCN activity of BBA, even if their fractions are significantly less than the organic fraction (Iinuma et al., 2007; Roberts et al., 2002).

Heterogeneous OH oxidation of organic aerosol can initiate reactions that result in the production of oxidized polar functional groups that can reduce the particle's surface tension (George et al., 2009) and increase water solubility (Suda et al., 2014), enabling greater water uptake and CCN activity. For example, Broekhuizen et al. (2004) demonstrated that unsaturated fatty acid aerosol particles comprised of oleic acid became more CCN active in the presence of high exposures to O₃. In a follow-up study, Shilling et al. (2007) corroborated this finding, attributing the enhancement in CCN activity to a combination of an increase in water-soluble material and a decrease in surface tension of the aqueous droplet during activation. Petters et al. (2006) demonstrated that the CCN activity of model saturated and unsaturated OA compounds is enhanced following oxidation by OH and NO₃. George et al. (2009) showed that the hygroscopicity of model OA, bis-ethyl-sebacate (BES) and stearic acid was enhanced following oxidative aging by OH radicals, which was attributed to the formation of highly water-soluble oxygenated functional groups. The hygroscopicity of OH-impacted ambient biogenic SOA was shown to increase at higher OH exposures as a result of an increasing oxygen-to-carbon (O:C) ratio (Wong et al., 2011).

In an effort to better understand the influence of chemical aging on the CCN activity of BBA, recent studies have investigated the influence of oxidative aging on particle hygroscopicity of either particles generated in the laboratory from a specific emission source (Martin et al., 2013; Grieshop et al., 2009; Novakov and Corrigan, 1996) or particles collected in the field (Rose et al., 2010; Gunthe et al., 2009), which may include multiple emission sources. While field-collected particle studies of hygroscopic growth and cloud formation are advantageous because they capture the chemical and physical complexity of ambient aerosol, they lack the specificity and control of laboratory studies in order to fully understand the fundamental physico-chemical processes that govern cloud formation. Martin et al. (2013) investigated the impact of photo-oxidation on the hygroscopicity of wood burning particles and found that after several hours of aging in a smog chamber there was a general enhancement in κ ; however, this was attributed to both condensation of oxidized organic or inorganic matter and oxidation of the particulate matter itself. However, the effects of OH-initiated oxidation on the hygroscopicity of BBA particles have not been examined systematically. In this work, we investigate the effects of heterogeneous OH oxidation of laboratory-generated BBA surrogate particles on the particles' hygroscopicity. Here, κ is evaluated for several pure-component and multicomponent aerosol particles containing both sparingly soluble and

highly water-soluble compounds, representing the range and complexity of atmospheric aerosol in regards to hygroscopicity and chemical composition. κ is evaluated as a function of OH exposure (i.e., $[\text{OH}] \times \text{time}$) and O_3 exposure using a custom-built aerosol flow reactor (AFR) coupled to a CCNc. The chemical aging effects on the CCN activity of internally mixed and organic-coated inorganic particles are presented.

2 Materials and methods

2.1 Aerosol generation, flow conditions, and measurement

Surrogate polydisperse BBA particles were generated by atomizing 1 wt % aqueous solutions of single-component particles LEV, MNC, KS, and particle mixtures of LEV:MNC:KS in 1:1:0, 0:1:1, 1:0:1, 1:1:1, and 1:0.03:0.3 mass ratios in a flow of ultra-high purity (UHP) N_2 using a commercial atomizer (TSI Inc. model 3076). To simulate the partitioning of MNC from the gas phase to the particulate phase, first reagent MNC was heated (up to $\sim 70^\circ\text{C}$) and volatilized, and then condensed onto KS seed particles. Growth of the KS seed particles by MNC condensation was achieved by gradually cooling the mixed MNC–KS flow downstream of the heating section before entering the flow reactor. The atomized particles were dried by passing the atomized flow through two diffusion dryers prior to entering the AFR. After exiting the AFR, the particles were subsequently dried in two additional diffusion dryers, where the overall sample flow $\text{RH} \leq 5\%$, before the size analysis and CCN activity measurements. This second drying stage was included in the experimental setup because the derivation of κ requires knowledge of dry particle size. The dry particle size distribution was determined with a differential mobility analyzer (DMA, TSI Inc. model 3081) and a condensation particle counter (CPC, TSI Inc. model 3772), and sampled at a total flow rate of 1.3 standard liters per minute (standard L min^{-1}). Number-weighted mean particle diameters, \overline{D}_p , for all of the particles investigated in this study ranged from ~ 40 to 150 nm.

2.2 OH generation, flow conditions, and measurement

OH radicals were generated via O_3 photolysis in the presence of water vapor in a 60 cm long and 5 cm inner diameter (i.d.) temperature-controlled Pyrex flow reactor as shown in Fig. 1 (Slade and Knopf, 2013; Kessler et al., 2010; George et al., 2009). O_3 was produced by flowing 2–25 sccm (standard cubic centimeters per minute) of UHP O_2 through an O_3 -producing lamp (Jelight model 600; emission wavelength $\lambda = 185$ nm). O_3 concentrations ranged from 250 ppb to 20 ppm and were monitored throughout the experiment using an O_3 photometric analyzer (2B Technologies model 202), which sampled at ~ 850 sccm. An O_3 denuder con-

taining a Carulite 200 catalyst was connected to the outlet of the AFR to convert O_3 to O_2 before entering the aerosol charge neutralizer and other sensitive instrumentation. A 50–600 sccm flow of UHP N_2 was bubbled in a 500 mL Erlenmeyer flask filled with distilled/deionized Millipore water (resistivity $> 18.2 \text{ M}\Omega \text{ cm}$) to generate humidified conditions in the AFR. The RH for all of the experiments was measured with an RH probe (Vaisala model HM70) and varied from 30 to 45 %. The humidified and O_3 flows were mixed in a 4.5 L glass vessel before entering with the particles into the AFR. The mixed $\text{N}_2/\text{O}_2/\text{O}_3/\text{H}_2\text{O}$ and particle flow was then passed over a 60 cm O_3 -free quartz tube containing a 60 cm long mercury pen-ray lamp ($\lambda > 220$ nm) to photolyze O_3 . The lamp was cooled with a flow of compressed air. Total flow rates in the flow reactor ranged from ~ 2.2 to 3 standard L min^{-1} , corresponding to a range in residence times of 26–39 s. Flows were laminar, with Reynolds numbers between 60 and 80. OH concentrations were determined by applying a photochemical box model validated based on isoprene loss measurements in the presence of OH as described previously (Slade and Knopf, 2013; George et al., 2009). OH concentrations ranged from $\sim 0.2 \times 10^{10}$ to 2×10^{10} molecule cm^{-3} and were varied by changing either RH or $[\text{O}_3]$. As previous studies have indicated, neither UV light nor O_3 introduction in this manner leads to particle degradation or a significant change in particle mass or chemistry (George et al., 2009; Kessler et al., 2010; Slade and Knopf, 2013). The temperature inside the flow reactor was maintained near 298 K by a cooling jacket. A slight temperature gradient of $\sim 3^\circ\text{C}$ from the leading edge of the sheath flow tube containing the lamp to the inner walls of the AFR was observed, but has no significant effect on $[\text{OH}]$. OH equivalent atmospheric exposures were determined from the product of the residence time in the AFR and applied $[\text{OH}]$, which was then normalized to a daily averaged ambient $[\text{OH}] = 2 \times 10^6$ molecule cm^{-3} . Using this method allowed varying atmospheric OH exposures equivalent to < 1 day up to ~ 1 week. At the given $[\text{OH}]$, residence time, total pressure of 1 atm, and particle sizes, we assume that OH mass transfer to the particles is sufficiently fast to maximize the exposure. At 40 % RH, the reactive uptake coefficient, γ , of LEV+OH would be 0.65 for atmospheric OH concentrations (Slade and Knopf, 2014). However, the presence of higher $[\text{OH}]$ in the AFR decreases γ to ~ 0.2 (Slade and Knopf, 2013). OH diffusion impacts γ by only $\sim 7\%$ (Fuchs and Sutugin, 1970), implying that OH exposure is not diffusion limited. At $\text{RH} > 15\%$, MNC is less reactive with OH, exhibiting $\gamma < 0.07$ due to competitive co-adsorption of water and OH (Slade and Knopf, 2014). Similar suppressions in gas uptake, due to competitive adsorption processes, have been observed in the case of OH and NO_3 uptake by BBA surrogate films (Slade and Knopf, 2013; Knopf et al., 2011), O_3 uptake by benzo[a]pyrene in the presence of water vapor (Pöschl et al., 2001), and O_3 and NO_2 uptake by benzo[a]pyrene-coated soot (Springmann et al., 2009; Kaiser et al., 2011).

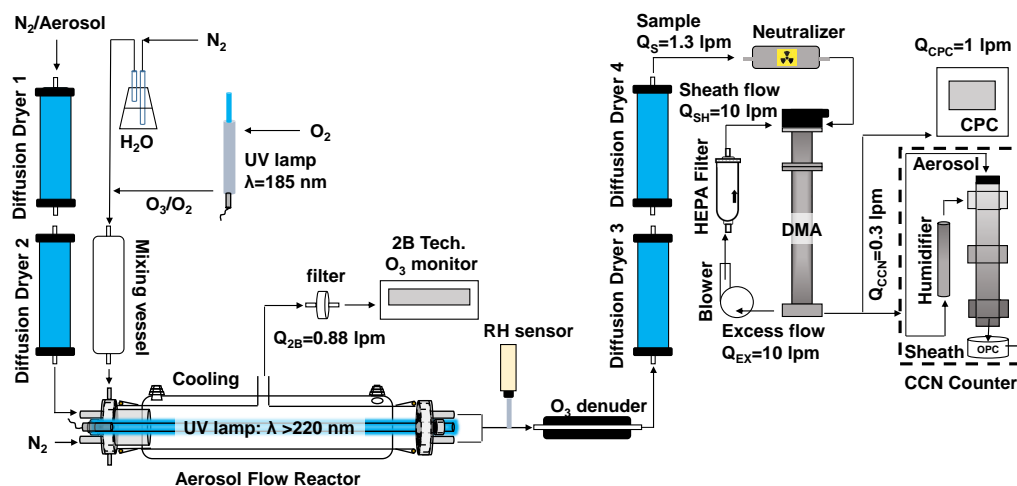


Figure 1. Schematic illustration of the experimental setup to examine the effect of OH and O₃ oxidation on the CCN activity of single-component and multicomponent biomass burning aerosol surrogate particles. From top left to bottom right: aerosol generation and drying stage, O₃ production and humidification (mixing vessel), the aerosol flow reactor, O₃-free ultraviolet lamp and O₃ monitor, relative humidity probe (RH sensor), O₃ denuder, second drying stages, aerosol sizing by the DMA and particle counting by the CPC, and determination of the CCN activity by the CCNc.

The presence of higher [O₃] may further decrease the OH reactivity of OA (Renbaum and Smith, 2011). Under the applied experimental conditions, the multiphase reaction kinetics involving highly viscous organic material are likely limited by surface–bulk exchange (Arangio et al., 2015; Slade and Knopf, 2014).

2.3 CCN measurements

The CCNc and operating conditions are described in more detail in Mei et al. (2013a). CCN activity data were acquired following procedures similar to previous studies (Petters and Kreidenweis, 2007; Petters et al., 2009), whereby the dry particle diameter is scanned while keeping the CCN chamber supersaturation fixed. A more detailed description of this approach is given in Petters et al. (2009). Briefly, particles first passed through a Kr-85 aerosol neutralizer (TSI 3077A), were size-selected using a DMA (TSI 3081), and processed in a CCNc (Droplet Measurement Technologies, Inc., single-column CCNc) (Roberts and Nenes, 2005; Lance et al., 2006; Rose et al., 2008), while in tandem the total particle concentration was measured with a CPC. The CCNc was operated at a 0.3 standard L min⁻¹ total flow rate and 10 : 1 sheath-to-sample flow rate ratio. The total sample flow rate, which includes a 1 standard L min⁻¹ CPC flow rate, was 1.3 standard L min⁻¹, and a 10 : 1.3 sheath-to-sample flow rate ratio was applied for the DMA. The temperature gradient in the CCNc column was set by custom-programmed Labview software and operated at $\Delta T = 6.5, 8, 10,$ and 12 K, corresponding to chamber supersaturations $S = 0.2, 0.27, 0.35,$ and 0.425% , based on routine calibrations applying atomized ammonium sulfate particles. The temperature gradient was stepped successively, from 6.5 to 12 K and in re-

verse. Each temperature gradient was maintained for a total of 14 min to allow an up and down scan of the particle size distribution by the DMA. The aerosol size distributions and size-resolved CCN concentrations were acquired by applying an inversion method described in Collins et al. (2002), which implicitly accounts for multiply charged particles. The ratio of the aerosol size distribution and CCN size distribution provided size-resolved CCN activated fractions (i.e., the fraction of particles that become CCN at a given supersaturation and particle size).

2.4 Hygroscopicity and CCN activity determination

The hygroscopicity and CCN activity can be described by κ -Köhler theory (KT) (Petters and Kreidenweis, 2007), which relates dry and wet particle diameter to the particle's critical supersaturation (RH above 100 %, at which the particle grows to a cloud droplet size) based on a single hygroscopicity parameter, κ . In κ -Köhler theory, the water vapor saturation ratio over an aqueous solution droplet as a function of droplet diameter, $S(D)$, is given by

$$S(D) = \frac{D^3 - D_d^3}{D^3 - D_d^3(1 - \kappa)} \exp\left(\frac{4\sigma M_w}{RT\rho_w D}\right), \quad (1)$$

where D is wet particle diameter, D_d is dry particle diameter, σ is droplet surface tension, M_w is the molecular weight of water, R is the universal gas constant, T is temperature, and ρ_w is density of water. κ ranges typically from ~ 0.5 to 1.4 for hygroscopic inorganic species and from ~ 0.01 to 0.5 for less hygroscopic organic species; $\kappa = 0$ represents an insoluble but wettable particle, and thus Eq. (1) reduces to the Kelvin equation (Petters and Kreidenweis, 2007).

An alternative, approximate expression for determining κ is given as follows (Petters and Kreidenweis, 2007):

$$\kappa = \frac{4A^3}{27D_d^3 \ln^2 S_c}, \quad (2)$$

where

$$A = \frac{4\sigma_{s/a}M_w}{RT\rho_w}. \quad (3)$$

S_c represents the critical supersaturation, i.e., point of supersaturation where more than 50 % of the initial dry particles are activated to CCN. Here, we assume $\sigma_{s/a}$ is equivalent to that of water. While aqueous solutions of LEV and KS exhibit surface tensions approximately equal to the surface tension of water (Tuckermann and Cammenga, 2004; Tuckermann, 2007), to our knowledge no previous surface tension measurements of MNC aqueous solutions have been made. Our assumption applying the surface tension of water at all OH exposures could result in an overestimation of κ since the presence of surface-active organics can decrease $\sigma_{s/a}$ (George et al., 2009; Schwiier et al., 2012; Nozière et al., 2014; Harmon et al., 2013). We do not have surface tension data of the different mixtures applied in this study. However, we anticipate that increasing OH exposure may decrease $\sigma_{s/a}$, thus enhancing the particle's CCN activity as demonstrated in George et al. (2009) and Harmon et al. (2013).

Hygroscopic growth of compounds exhibiting moderate to weak solubility in water can be limited by their low water solubility (Petters and Kreidenweis, 2008), and thus cannot be treated as either fully dissolvable or insoluble substances. A theoretical treatment of κ , which includes solubility limitations, has been detailed in Petters and Kreidenweis (2008). Here,

$$\kappa = \varepsilon_i \kappa_i H(x_i) \quad (4)$$

$$H(x_i) = \begin{cases} 1 & \text{if } x_i \geq 1 \\ x_i & \text{if } x_i < 1 \end{cases}, \quad (5)$$

where ε is the volume fraction of the solute i in the dry particle. κ_i is the theoretical κ of solute i in the absence of solubility limitations and is given by

$$\kappa_i = \frac{\nu \rho_i m_w}{\rho_w m_i}, \quad (6)$$

where ν is the Van't Hoff factor, ρ_i is the density of the solute, ρ_w is the density of water, m_i is the molar mass of the solute, and m_w is the molar mass of water. x_i is defined as the dissolved volume fraction of the solute (Petters and Kreidenweis, 2008) and given as

$$x_i = C_i \frac{V_w}{V_i}, \quad (7)$$

where C_i is the water solubility of the solute, expressed as the solute volume per unit water volume at equilibrium with saturation, and V_i is the volume of the solute. For complete dissociation, x_i is equal to unity. The parameters listed in Table 1 were used in predicting κ .

3 Results and discussion

3.1 CCN activity of BBA surrogate particles

Exemplary activated fractions, i.e., fractions of initial dry particle sizes activated to CCN, for LEV, MNC, KS, and the ternary particle mixtures at a chamber supersaturation of 0.425 %, are shown in Fig. 2. The activated fraction curves were fit to a cumulative Gaussian distribution function as described in detail previously (Petters et al., 2009):

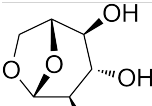
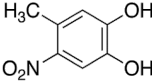
$$f(x) = \frac{1}{2} \operatorname{erfc} \left(\frac{x}{\sqrt{2}} \right), \quad (8)$$

where $x = (D_d - D_{d,50})/\sigma_D$. In the fitting procedure, D_d is the dependent variable and $D_{d,50}$ and σ_D are adjustable parameters to minimize the root mean square error between $f(x)$ and the data. $D_{d,50}$ is the dry diameter interpreted as being where 50 % of the dry particles have activated into cloud droplets, also referred to as the critical particle diameter, $D_{p,c}$.

KS particles exhibit the smallest particle activation diameter of ~ 50 nm, followed by LEV particles at ~ 75 nm, and MNC particles at ~ 210 nm at $S = 0.425$ %. In this study, κ is derived from Eq. (2), where S is evaluated at 0.2, 0.27, 0.35, and 0.425 % is used in place of S_c , and D_d is the determined $D_{p,c}$. At lower S , the activated fraction curves are shifted to larger sizes since the smaller particles do not activate at lower S .

Table 2 lists the derived κ values for all of the particle types employed in this study in comparison to literature values. The reported uncertainties in κ are $\pm 1\sigma$ from the mean κ derived at each S . The derived κ values for LEV and KS are consistent with κ for LEV and KS given in the literature. The critical diameter of LEV (~ 70 nm at $S = 0.425$ %) is in good agreement with the critical diameter of LEV measured by Petters and Kreidenweis (2007) at the same S . κ ranges from 0.149 (± 0.008) to 0.176 (± 0.009) for LEV over all S , in agreement with the humidified tandem DMA (HT-DMA) derived $\kappa = 0.165$ (Carrico et al., 2010). Within experimental uncertainty, κ for KS is in agreement with the value derived in Carrico et al. (2010), but exhibits a marginal increase as a function of S , possibly due to an increasing van't Hoff factor at higher S , similar to ammonium sulfate. To our knowledge, no previous hygroscopicity measurements of MNC have been made. κ ranges from 0.008 (± 0.002) to 0.013 (± 0.003) for MNC. However, κ could not be derived for MNC at $S = 0.2$ %, given the applied aerosol size distribution. In other words, the $D_{p,c}$ is likely too large, and

Table 1. Chemical properties of the different particle types investigated in this study and the parameters used in predicting κ .

Molecule	Structure	M (g mol ⁻¹)	ρ (g cm ⁻³)	Solubility (g L ⁻¹)	C_i	ν
Levoglucosan		162.14	1.69	1000	0.592	1
4-methyl-5-nitrocatechol		169.13	1.5	4.8 ^a	0.003	1
K ₂ SO ₄		174.26	2.66	11	0.042	2 ^b

^a Estimated using the US Environmental Protection Agency's Estimation Program Interface (EPI) suite (EPI, 2015). ^b Taken from the reported Van't Hoff factor in Low (1969) for (NH₄)₂SO₄ assuming a solution droplet molality of approximately 0.2.

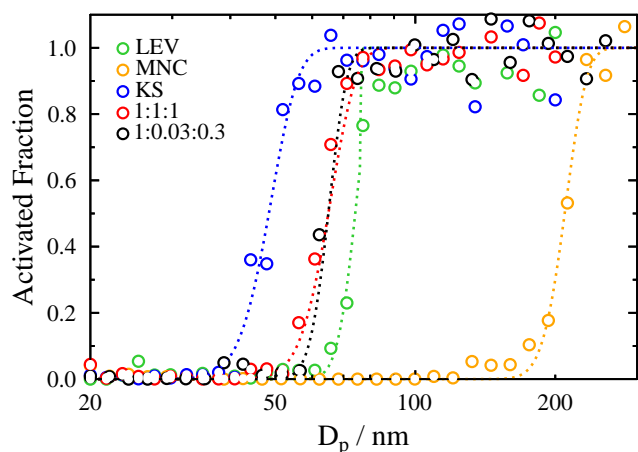


Figure 2. Activated fractions, i.e., fractions of the number of particles at a given particle size activated to CCN as a function of the initial dry particle diameter, for LEV (green), MNC (orange), KS (blue), 1 : 1 : 1 (red) and 1 : 0.03 : 0.3 (black) particles at $S = 0.425\%$. The dotted lines correspond to the fits applying Eq. (8).

the scanned particle size range is not sufficient to give the complete activation curve. As a result, the $D_{p,c}$ could not be reliably derived. For comparison, humic-like substances (HULIS), which is known to contain nitrocatechols (Claeys et al., 2012), exhibits a κ value of 0.05 (Carrico et al., 2010). In addition, κ for NO₃ oxidized oleic acid particles, comprising similar chemical functionalities as MNC (i.e., nitrogen oxides and conjugated double bonds), is ~ 0.01 (Petters et al., 2006).

On average, κ for all of the binary and ternary mixed particles range from 0.111 (± 0.010) to 0.373 (± 0.034). Due to constraints in water uptake and water solubility, mixed particles comprising a significant fraction of MNC (i.e., 1 : 1 : 0, 0 : 1 : 1, 1 : 1 : 1) exhibit relatively lower κ than the 1 : 0 : 1 mixture. The 1 : 0.03 : 0.3 ternary-component particles exhibit a slightly lower κ compared to the other particle mixtures, due to the relatively low KS content. It is not entirely

clear why the particles exhibit lower κ at $S = 0.2\%$. This implies that either the supersaturation used to derive κ was artificially high, the van't Hoff factor is lower, or limitations in solubility are more pronounced at this lower supersaturation than at higher supersaturations. The calibration data applying ammonium sulfate particles yield a variability in the derived supersaturation at $S = 0.2\%$ of $\sim 5\%$, which still results in less variability in the derived κ values at that supersaturation compared to what was observed.

As listed in Table 2, the derived κ values are reasonably predicted by applying the volume mixing rule (Petters and Kreidenweis, 2007):

$$\kappa = \kappa_{\text{Org}} \times \varepsilon_{\text{Org}} + \kappa_{\text{Inorg}}(1 - \varepsilon_{\text{Org}}), \quad (9)$$

where κ_{Org} and κ_{Inorg} are the κ values of the organic and inorganic particles, respectively, and ε_{Org} is the organic volume fraction of the particles. However, the quality of the estimate depends on whether the effects of solubility are to be included. For example, applying the experimentally derived κ of MNC particles in the volume mixing rule results in a significant underprediction of κ for the 1 : 1 : 0, 0 : 1 : 1, and 1 : 1 : 1 particle mixtures. This deviation in κ suggests that water uptake by the pure-component MNC particles is mechanistically different than water uptake by the mixed particles, which contain a significant MNC volume fraction. The volume mixing rule is applicable over a range of mixtures and hygroscopicity. However, when the particles contain both soluble and sparingly soluble compounds, predicted κ can deviate significantly from derived κ (Petters and Kreidenweis, 2008). MNC is significantly less water-soluble than pure LEV and KS. During CCN activation, the most water-soluble component preferentially dissolves, enhancing the solute effect in the Köhler equation. Since water-soluble components in aerosol particles can retain greater liquid water content during water uptake, the less water-soluble component can more easily dissolve (Bilde and Svenningsson, 2004; Abbatt et al., 2005; Shantz et al., 2008; Petters and Kreidenweis, 2008). This solubility constraint in the volume mixing rule is described in more detail in Petters and Krei-

Table 2. Tabulated experimentally derived hygroscopicity parameters, κ , for the various particle types investigated in this study before oxidation.

Compound	κ^a				κ^b	κ^c
	0.2 %	0.27 %	0.35 %	0.425 %		
LEV	0.149 (± 0.008)	0.175 (± 0.010)	0.172 (± 0.009)	0.176 (± 0.009)	0.188	0.165 ^d 0.208 (± 0.015) ^e
KS	0.525 (± 0.052)	0.575 (± 0.026)	0.563 (± 0.024)	0.538 (± 0.074)	0.55	0.52 ^d
MNC	N/A	0.013 (± 0.003)	0.012 (± 0.005)	0.008 (± 0.002)	0.16	
LEV : MNC : KS	κ^a				κ^b	
Mass ratio	0.2 %	0.27 %	0.35 %	0.425 %		
1 : 1 : 0	0.114 (± 0.010)	0.143 (± 0.016)	0.131 (± 0.005)	0.137 (± 0.009)	0.173	
1 : 0 : 1	0.310 (± 0.047)	0.360 (± 0.031)	0.373 (± 0.029)	0.373 (± 0.034)	0.329	
0 : 1 : 1	0.239 (± 0.030)	0.336 (± 0.068)	0.331 (± 0.014)	0.322 (± 0.015)	0.300	
1 : 1 : 1	0.216 (± 0.029)	0.255 (± 0.012)	0.270 (± 0.013)	0.268 (± 0.013)	0.256	
1 : 0.03 : 0.3	0.209 (± 0.010)	0.233 (± 0.008)	0.232 (± 0.005)	0.234 (± 0.022)	0.241	

^a This study. Reported uncertainties are 1σ from the mean in the derived κ .

^b Predicted values applying the volume mixing rule without solubility limitations.

^c Literature-reported values.

^d Carrico et al. (2010).

^e Petters and Kreidenweis (2007).

denweis (2008). As a result and depending on the volume fraction of the sparingly soluble compounds in the particle, the peak of the Köhler curve may occur at a sufficiently large droplet size when all compounds, including the sparingly soluble compounds, are completely dissolved. The same can be applied here for the mixtures containing an appreciable MNC volume fraction. The water solubility of MNC is approximated as $C = 0.003$, which is categorized as sparingly water-soluble (Petters and Kreidenweis, 2008). To verify whether MNC behaves as if it is infinitely soluble in a solution with KS, Fig. 3 shows derived Köhler curves of pure MNC and mixtures containing variable KS volume fractions and the MNC dissolved fraction, x_{MNC} . In Fig. 3, the critical supersaturation, i.e., the maximum in the Köhler curve, decreases with increasing KS volume fraction. Accordingly, the MNC dissolved fraction increases with an increasing KS volume fraction. At a KS volume fraction of $\sim 36\%$ (MNC volume fraction of $\sim 64\%$) indicated by the orange curves in Fig. 3, the maximum in the Köhler curve corresponds to $x_{\text{MNC}} \approx 1$, implying that CCN activation is not limited by MNC solubility. This MNC volume fraction corresponds to the 1 : 1 by mass MNC : KS particles, which suggests that for this particular mixture, MNC behaves as if there are no solubility limitations during CCN activation (i.e., infinitely soluble, equivalent to $C = \infty$) and κ of MNC can be predicted using Eq. (6). This result is consistent with the 1 : 1 : 1 by mass LEV : MNC : KS particles. In the presence of LEV, alone, MNC remains slightly insoluble during CCN activation.

Figure 4 shows the predicted κ plotted against experimentally derived κ for all of the particle mixtures and S applied in this study. κ was predicted by applying the volume mixing rule under three different scenarios: (1) calculated from ex-

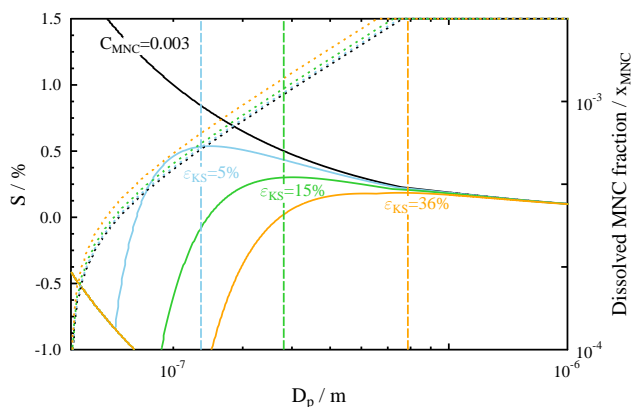


Figure 3. Example Köhler curves (solid lines) calculated from Eq. (1) for pure MNC (black), MNC mixed with 5% (blue), 15% (green), and 36% (orange) by volume KS. The dotted lines are the dissolved fractions of MNC, x_{MNC} , calculated from Eq. (7), corresponding to the different Köhler curves. The vertical dashed lines indicate the maxima of the different Köhler curves. The dry diameter applied is 110 nm.

perimentally derived single-component κ ($\kappa = \text{limit}$; color-scale symbols), (2) calculated from Köhler theory ($\kappa = \text{KT}$; gray-scale symbols), and (3) predicted from Eq. (6), which assumes no solubility limitations (i.e., $C = \infty$; horizontal lines). For all particle mixtures containing equal by mass MNC (i.e., 1 : 1 : 0, 0 : 1 : 1, and 1 : 1 : 1), applying the experimentally derived single-component κ underpredicts the experimentally derived κ of the mixtures. Note that when assuming solubility limitations, κ could not be predicted at $S = 0.2\%$ for the mixtures containing MNC since κ for

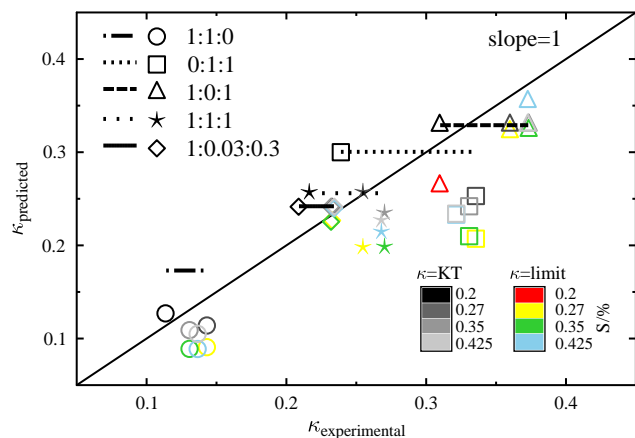


Figure 4. Predicted κ as a function of experimentally derived κ at different supersaturations (S) for the binary and ternary particle mixtures of LEV, MNC, and KS. κ is predicted by applying the volume mixing rule and based on single-component experimentally derived κ at each S including solubility limitations ($\kappa = \text{limit}$; color scale), κ calculated from Köhler theory ($\kappa = \text{KT}$; gray scale), and κ assuming no solubility limitations (horizontal lines). Note that the horizontal lines span the range of experimentally derived κ . The black diagonal line represents a slope of 1 in the derived vs. predicted κ . The LEV : MNC : KS mass ratios are indicated in the legend for 1 : 1 : 0 (circle), 0 : 1 : 1 (square), 1 : 0 : 1 (triangle), 1 : 1 : 1 (star), and 1 : 0.03 : 0.3 (diamond).

MNC, alone, could not be derived experimentally at that supersaturation. As discussed previously, this underprediction is due to the enhancement in MNC water solubility when in the presence of water-soluble LEV and KS, which is not accounted for applying the experimentally derived single-component κ . Applying Köhler theory results in better agreement with the experimentally derived κ , particularly for the 1 : 1 : 0 particle mixture. Predicted κ assuming no solubility limitations results in an overprediction for the 1 : 1 : 0 particle mixture, but is in best agreement with the experimentally derived κ for all other mixtures. The ability to predict experimentally derived κ of the mixtures applying Köhler theory depends on the solubility and volume fractions of the different particle components, which have not all been measured. The solubility of MNC was estimated from the US Environmental Protection Agency's Estimation Program Interface (EPI) suite (EPI, 2015). Applying this estimated solubility results in an underprediction in the 0 : 1 : 1 and 1 : 1 : 1 κ , but is in best agreement for the 1 : 1 : 0 particle mixture. These results support the finding that the volume mixing rule is most accurate when accounting for the changes to water solubility when the components are mixed. In the presence of LEV, MNC remains slightly insoluble. However, in the presence of KS, MNC behaves as if there are no solubility limitations during CCN activation.

3.2 CCN activity of single-component BBA surrogate particles exposed to OH

Surrogate single-component BBA particles were oxidized in the presence of O_3 (mixing ratio, $\chi_{\text{O}_3} = 0.76\text{--}20$ ppm) and in the presence of OH radicals ($0.2 \times 10^{10}\text{--}2 \times 10^{10}$ molecule cm^{-3}), corresponding to < 1 day up to ~ 1 week of a 12 h daytime OH exposure at $[\text{OH}] = 2 \times 10^6$ molecule cm^{-3} . κ as a function of O_3 exposure is presented in the Supplement. Upon exposure to OH, both LEV and MNC particles exhibited significant chemical erosion due to molecular fragmentation and volatilization (George et al., 2009; Kessler et al., 2010; Slade and Knopf, 2013). Figure 5 shows the evolution of LEV and MNC particle volume in the presence of OH, V (Hg lamp on, with O_3), normalized to the initial particle volume just before switching on the Hg lamp, V_0 (Hg lamp off, with O_3), as a function of OH exposure. Following OH exposure, the average decrease in particle volume for all OH exposures for LEV and MNC particles was $36(\pm 7)$ and $19(\pm 7)\%$, respectively. In general, OH exposure led to an increase in LEV modal particle diameter and a decrease in MNC modal particle diameter. The increase in LEV modal particle diameter in combination with a decrease in total particle volume suggests the smallest LEV particles experienced the most chemical erosion. Occasionally, a second smaller size mode developed following OH oxidation of pure MNC particles. While the exact mechanism for the formation of the smaller mode is not clear, we speculate that OH oxidation of gas-phase MNC could lead to in situ particle formation in the flow reactor. Particle size is not expected to alter κ directly unless a change in particle size coincides with a change in particle composition. Given that there are two different particle populations and presumably two different particle compositions following OH oxidation of MNC, the newly formed particles may affect the derived κ . Clearly, more careful control and study of the particle size distribution are needed to resolve the impacts of volatilization, but are beyond the scope of this study.

κ was determined as a function of OH exposure and S for the single-component organic particles LEV and MNC as shown in the top panels of Fig. 6. The bottom panels of Fig. 6 correspond to the critical particle diameter as a function of OH exposure. It should be noted that the critical particle diameter decreases with increasing S . For the same exposure, smaller particles become more oxidized due to their larger effective surface area to volume ratio. As demonstrated in Fig. 6 for both LEV and MNC, at a fixed OH exposure, the largest κ corresponds to the smallest critical particle diameter. While it is clear that κ depends on the particle size at a fixed OH exposure, we are interested in the resulting changes to κ due to increasing OH exposure at the applied S . For both LEV and MNC, the trend in κ as a function of OH exposure does not significantly deviate for the applied particle sizes. For LEV particles, κ at the lowest OH exposure is not significantly different to κ derived at the highest OH exposure.

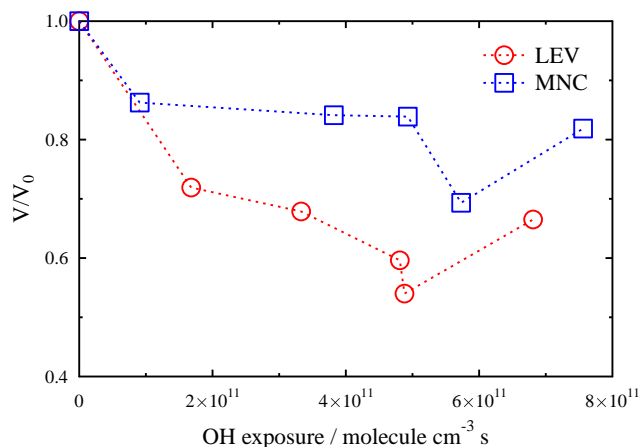


Figure 5. LEV and MNC particle volume change as a function of OH exposure. The measured particle volume in the presence of OH (V ; Hg lamp on, with O_3) is normalized to the measured particle volume in the absence of OH (V_0 ; Hg lamp off, with O_3).

Conversely, MNC κ increases significantly from ~ 0.01 to ~ 0.1 with increasing OH exposure at all applied S .

The reactive uptake, condensed-phase reaction products, and volatilized reaction products resulting from heterogeneous OH oxidation of LEV are well documented (Kessler et al., 2010; Hoffmann et al., 2010; Bai et al., 2013; Slade and Knopf, 2013, 2014; Zhao et al., 2014). However, there are no direct measurements of its CCN activity following OH exposure. Kessler et al. (2010) showed that following OH exposure, particle volatilization accounts for a $\sim 20\%$ by-mass loss of LEV. This suggests that the majority of the reaction products, which include carboxylic and aldehydic species (Bai et al., 2013; Zhao et al., 2014), remain in the condensed phase. Although volatilization due to high OH exposures has been linked to an increase in the critical supersaturation and thus suppression in the CCN activity of oxidized squalane particles (Harmon et al., 2013), the results here suggest that, regardless of volatilization, the condensed-phase reaction products are just as or somewhat more active CCN than pure LEV. On average, there is only a slight increase in κ for LEV particles, with increasing OH exposure as indicated by the positive slope in the linear fit to the data at all applied S . Such an incremental enhancement in κ may be a result of similar κ between LEV and its oxidation products. The hygroscopicity of several carboxylic acids that may represent levoglucosan OH oxidation products, including malonic, glutaric, glutamic, succinic, and adipic acid, exhibits κ values between 0.088 and 0.248 (Petters and Kreidenweis, 2007), similar to κ of oxidized and pure LEV. Furthermore, the hygroscopicity of organic compounds containing hydroxyl functionalities similar to LEV or carboxylic groups are nearly equivalent (Suda et al., 2014). We also cannot rule out that volatilization, while reducing particle mass, also removes newly formed reaction products from the

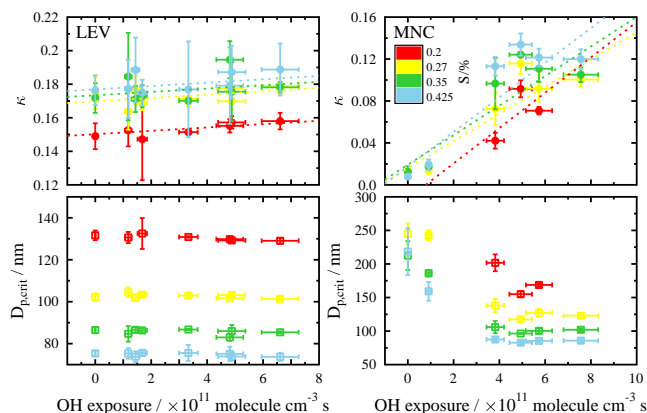


Figure 6. Derived κ (top) and critical particle diameter (bottom) for LEV and MNC particles are shown as a function of OH exposure. As indicated in the legend, the colors represent the different supersaturations (S) accessed during this study. The vertical error bars represent $\pm 1\sigma$ from the mean of the data acquired at a given OH exposure and S . Horizontal error bars correspond to the uncertainty in the OH exposure based on a $\pm 5\%$ drift in RH over the sampling period. The dotted lines show the best linear fit to the OH exposure data as a function of S .

aerosol phase, leaving the parent organic (i.e., LEV) and thus κ unchanged.

The CCN activity of MNC aerosol particles increases with OH exposure as shown in the top right panel of Fig. 6. MNC becomes more CCN active with increasing OH exposure and κ transitions from ~ 0.01 in the absence of OH to ~ 0.1 for OH exposures equivalent to a few days in the atmosphere. Further exposure ($\geq 4 \times 10^{11}$ molecules $\text{cm}^{-3} \text{s}^{-1}$) does not significantly enhance MNC κ , which suggests that MNC or the particle surface is fully oxidized (Slade and Knopf, 2014) and that the reaction products reach a maximum in κ . Similar enhancements in κ and subsequent constant κ values with increasing OH exposure have been observed for organic aerosol with initially low hygroscopicity (George et al., 2009; Lambe et al., 2011). For example, George et al. (2009) observed that κ of BES increased from ~ 0.008 to ~ 0.08 for an OH exposure of $\sim 1.5 \times 10^{12}$ molecules $\text{cm}^{-3} \text{s}^{-1}$, and κ of stearic acid increased from ~ 0.004 to ~ 0.04 due to an OH exposure of $\sim 7.5 \times 10^{11}$ molecules $\text{cm}^{-3} \text{s}^{-1}$.

The enhancement in MNC κ following OH exposure may be linked to the formation of more hydrophilic chemical functionalities. Strongly linked to enhancements in OA hygroscopicity are larger O:C ratios (Massoli et al., 2010; Lambe et al., 2011; Mei et al., 2013a, b; Suda et al., 2014). Neglecting the oxygen atoms in the -nitro functionality of MNC (Suda et al., 2014), the O:C ratio of pure MNC is ~ 0.29 , close to the lower end in O:C where transitions from low κ to high κ typically occur (Suda et al., 2014). The presence of -methyl, unsaturated, and -nitro functionalities are also linked to low hygroscopicity (Suda et al., 2014). As proposed in Slade and Knopf (2014) and observed for other

nitro-phenolic species, OH oxidation of MNC can favor removal of the -nitro functionality by electrophilic substitution of OH (Slade and Knopf, 2013; Di Paola et al., 2003; Chen et al., 2007). OH substitution at the -methyl position and addition to the double bonds is also possible (Anbar et al., 1966). OH addition to the -nitro or -methyl functionality would increase O : C to ~ 0.43 or ~ 0.5 , respectively. OH substitution at both positions would enhance O : C to ~ 0.67 . Suda et al. (2014) showed that hydroxyl-dominated OA with an O : C of less than ~ 0.3 has an apparent κ of $\leq 10^{-3}$. However, an increase in O : C to 0.4 or 0.6 due to the addition of hydroxyl, aldehydic, or carboxylic functionalities results in an enhanced κ of ~ 0.1 . Thus, small changes in O : C can significantly affect κ . Pure MNC is also sparingly soluble in water and thus κ is strongly dependent on its actual solubility, which can change depending on the oxidation level and the presence of other compounds having different solubility (Petters and Kreidenweis, 2008). Consequently, the conversion from low to high κ following OH oxidation is consistent with the addition of more hydrophilic functionalities and a molecular transition from sparingly soluble to sufficiently water-soluble. Interestingly, MNC, while having a 10 times smaller OH uptake coefficient compared to LEV at the same RH (Slade and Knopf, 2014), exhibits a greater change in κ than LEV following OH oxidation. Under dry conditions, we understand uptake is limited by surface–bulk processes (Arangio et al., 2015; Slade and Knopf, 2014). In that case, due to the low hygroscopicity and low water solubility of MNC, its viscosity may be sufficiently high that oxidation is limited to the particle surface. Consequently, MNC surface molecules may undergo several generations of oxidation as opposed to LEV, which is known to undergo a semi-solid to liquid-phase transformation at the same RH = 40 % (Mikhailov et al., 2009). However, assessing the effects of RH or bulk diffusivity on hygroscopicity following OH exposure is beyond the scope of the current work.

3.3 CCN activity of binary-component BBA surrogate particles exposed to OH

Binary-component particles consisting of LEV:MNC, LEV:KS, and MNC:KS in 1 : 1 mass ratios were exposed to OH and analyzed for their hygroscopicity as a function of OH exposure. The approach here is to determine whether the presence of more than one component can influence the hygroscopicity of another following OH and oxidation; i.e., are the observed changes in hygroscopicity of the pure-component particles following OH oxidation retained when mixed? Figure 7 shows κ and the critical particle diameter for the different binary aerosol mixtures as a function of OH exposure for each applied S . κ as a function of O_3 exposure is presented in the Supplement. The dotted and dashed lines in Fig. 7 display the predicted κ as a function of OH exposure using the volume mixing rule including and excluding MNC solubility limitations, respectively, based on the linear fits of

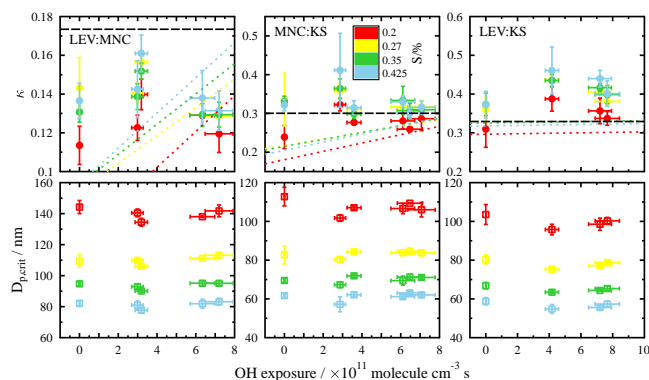


Figure 7. Derived κ (top) and critical particle diameter (bottom) for the binary-component particles with 1 : 1 mass ratios are shown as a function of OH exposure. As indicated in the legend, the colors represent the different supersaturations (S) accessed during this study. Error bars are calculated as in Fig. 6. The dotted lines are modeled κ using the volume mixing rule as a function of OH exposure applying the linear fit to the derived κ of pure MNC and LEV as a function of OH exposure (Fig. 6). The dashed black lines are the modeled κ using the volume mixing rule and assuming no solubility limitations.

κ as a function of OH exposure for pure LEV and MNC particles (Fig. 6) at each S . Modeled κ as a function of OH exposure excluding MNC solubility limitations (i.e., black dashed lines in Fig. 7) assumes that κ for MNC of the mixed particles is 0.16.

There are two important points to be made regarding the results from Fig. 7. (1) Hygroscopicity of the mixed particles is virtually unchanged as a function of OH exposure; i.e., while OH exposure significantly impacts MNC hygroscopicity alone, it does not significantly influence κ for the binary-component particles containing MNC as predicted by the volume mixing rule applying the single-component experimentally derived κ for LEV, MNC, or KS. (2) κ and the trend in κ with OH exposure are significantly underpredicted assuming MNC solubility limitations are applicable in the volume mixing rule (dotted lines in Fig. 7). As discussed previously and demonstrated in Fig. 3, the presence of either KS or LEV influences the extent that MNC solubility impacts particle activation. We have shown that MNC exhibits no solubility limitations for the volume fractions applied here. Larger MNC volume fractions are expected to have a greater influence on κ following OH exposure. The organic content of BBA was shown to dominate hygroscopic growth, in particular the water-soluble organic content (WSOC), which is largely levoglucosan (Dusek et al., 2011). Other studies have indicated that sparingly soluble organic compounds have limited importance in atmospheric aerosol CCN activity (Dusek et al., 2003; Gasparini et al., 2006; Ervens et al., 2005; Andreae and Rosenfeld, 2008), although they are, besides completely insoluble organic material, the most likely class of compounds susceptible to hygroscopic

changes following oxidation, due to their low water solubility. In other words, there is more room for an enhancement in the solute effect of sparingly soluble organic particles than there is for more water-soluble particles. Our results show that oxidative aging impacts on the hygroscopicity of pure-component particles can be vastly different if the particles are internally mixed with substances having different water solubility.

3.4 CCN activity of ternary-component BBA surrogate particles exposed to OH

Here we investigate the CCN activity of internally mixed LEV, MNC, and KS particles with 1 : 1 : 1 and with an atmospherically relevant mass ratio of 1 : 0.03 : 0.3 (LEV : MNC : KS) following exposure to OH. The results for the OH exposure are shown in Fig. 8 and κ as a function of O_3 exposure is presented in the Supplement.

Within the uncertainty of the derived κ values for the 1 : 1 : 1 and 1 : 0.03 : 0.3 ternary-component particles, their hygroscopicities are virtually unaffected by OH exposure, similar to the binary mixtures. However, on average the 1 : 1 : 1 particle mixture exhibits a slight enhancement in hygroscopicity. The predicted κ values for the 1 : 1 : 1 mixture, which include MNC solubility limitations (dotted lines), significantly underestimate κ , and only after removing these limitations (black dashed line) does the predicted κ agree with the experimentally derived κ . This is not surprising, given that the more water-soluble components LEV and KS are present at equal mass to MNC. Thus MNC behaves as if it is infinitely soluble during CCN activation. One possible explanation for the slight enhancement in κ with OH exposure, which differs from the binary mixed particles, is the presence of both MNC and LEV, which both exhibit enhancements in κ following OH oxidation. However, the range in derived κ at a given OH exposure is sufficiently large that, within experimental uncertainty, there is no significant trend in κ with OH exposure.

The WSOC, mostly LEV, is known to dominate the BBA volume fraction (Dusek et al., 2011). MNC constitutes $\leq 5\%$ by mass of the BBA organic fraction as determined from both field and lab chamber studies (Iinuma et al., 2010; Claeys et al., 2012). The remaining fraction can be largely composed of inorganic salts, including KS (Pósfai et al., 2003; Rissler et al., 2006). To simulate atmospheric BBA, we atomized a mixed aqueous solution of LEV, MNC, and KS in a mass ratio of 1 : 0.03 : 0.3 and determined its CCN activity unexposed and after exposure to OH and O_3 . The resulting κ of this mixture as a function of OH exposure is displayed in the top right panel of Fig. 8. As anticipated, since pure LEV shows little enhancement in CCN activity with OH exposure (Fig. 6) and dominates the volume fraction of this mixture, and KS is unreactive to OH, no enhancements in κ following OH exposure were observed. A similar observation was made from laboratory-controlled burns, whereby following

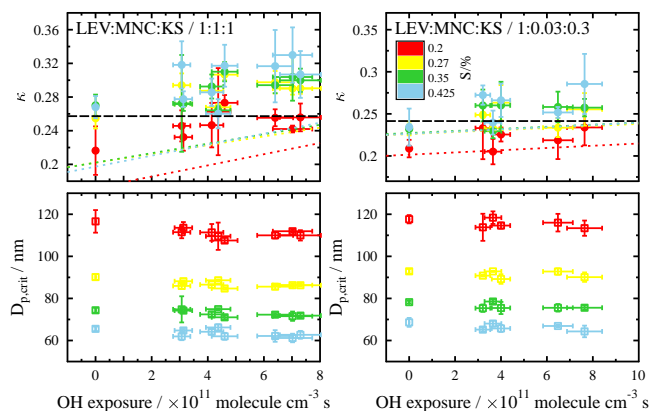


Figure 8. Derived κ (top) and critical particle diameter (bottom) for the ternary-component particles with LEV : MNC : KS mass ratios 1 : 1 : 1 (left) and 1 : 0.03 : 0.3 (right) are shown as a function of OH exposure. As indicated in the legend, the colors represent the different supersaturations (S) accessed during this study. The dashed black lines are calculated as in Fig. 7 and error bars and dotted lines are calculated as in Figs. 6 and 7, respectively.

several hours of photo-oxidation, there were very slight enhancements in κ of the particles (Martin et al., 2013). Larger enhancements in κ were observed only for the SOA particles generated from oxidative aging of gas-phase volatiles emitted during the controlled burns, in the absence of seed particles (Martin et al., 2013). This implies that photo-oxidative aging of BBA may contribute little to changes in its hygroscopicity, unless the entire aerosol population is comprised of SOA material (e.g., MNC). Furthermore, both predicted κ including solubility limitations and without solubility limitations are in agreement with the derived values. This is due to the low mass fraction of MNC present, which has sufficiently low impact on both the solubility and oxidation level of the mixed aerosol particles.

3.5 Mixing state effects on κ

Internally mixed organic–inorganic atmospheric aerosol particles can exhibit phase separations, i.e., a core-shell structure, which often contains an insoluble or solid inorganic core with a less viscous organic outer layer (Cruz and Pandis, 1998; Pósfai et al., 1998; Russell et al., 2002). The presence of an organic coating has been shown to impact CCN activity and water uptake (Cruz and Pandis, 1998; Abbatt et al., 2005; Garland et al., 2005), ice nucleation efficiency (Knopf et al., 2014; Wang et al., 2012; Baustian et al., 2012; Friedman et al., 2011; Möhler et al., 2008), and heterogeneous chemistry (Katrib et al., 2004; Gierlus et al., 2012; Knopf et al., 2007; Cosman et al., 2008). Because MNC originates from gas-phase chemical reactions, and its concentration determined in BBA particles, MNC must partition from the gas to the particulate phase. In this section, we investigate whether the mixing state of mixed MNC and KS particles

has an effect on its CCN activity following OH exposure by the application of MNC-coated particles in comparison to the atomized MNC : KS binary-component particles. For example, Abbatt et al. (2005) observed a complete deactivation in the CCN activity of ammonium sulfate particles when thickly coated with stearic acid.

The CCN activity of KS particles coated with MNC was derived as a function of the organic volume fraction ($V_{f,org}$) of MNC, and before and after OH exposure as shown in Figs. 9a–c. Figure 9a displays a color map of the dry KS particle size distribution evolution following exposure to MNC in the absence of OH, where time = 0 min is the point at which KS particle growth by MNC condensation begins. The 25th, 50th, and 75th percentiles of the number-weighted particle size distribution grew in size by ~ 20 nm as indicated by the red, black, and blue circles in Fig. 9a, respectively. For the 50th percentile, this corresponds to an enhancement in the MNC $V_{f,org}$ from 0 % at time = 0 min to ~ 70 % shortly after, close to the $V_{f,org}$ of the atomized MNC : KS binary-component particles of 64 %. The similar $V_{f,org}$ between the atomized and coated MNC-KS particles enables a direct inter-comparison of their hygroscopicity, since relatively larger MNC $V_{f,org}$ would bias towards lower κ and vice versa, as indicated in the colored dashed and dotted lines in Fig. 9b.

The particles' hygroscopicity was analyzed throughout the period of condensational growth as demonstrated in Fig. 9b and shown as the black circles. It is important to note that the particle size distribution is scanned (up and down voltage scans) at four different S (0.2, 0.27, 0.35, and 0.425 %) in ascending and descending order, a process that takes roughly 90 min. In contrast to the atomized binary-component particles, here KS particles grow due to MNC condensation over this experimental time period. Hence, the DMA and CCN capture the size distribution and CCN activity of a time-dependent and compositionally different particle population at each scan. The black line in Fig. 9b displays the steps in S over the course of the experiment. The first two κ values are of pure KS particles evaluated at $S = 0.2$ %. Subsequent κ values are of MNC-coated KS particles, which increase in $V_{f,org}$ with time. The change in $V_{f,org}$ with time is indicated by the red, black, and blue circles according to the 25th, 50th, and 75th percentiles of the particle population, respectively. $V_{f,org}$ allows one to compare derived κ with that predicted using the volume mixing rule. As previously discussed, the solubility limitations of pure MNC can be neglected when predicting κ of the atomized 1 : 1 mass ratio MNC : KS binary-component particles. To determine whether the solubility of MNC impacts the MNC-coated KS particles similarly to the atomized mixture, κ is predicted using the volume mixing rule and applying the experimentally derived pure MNC κ corresponding to a specific S (i.e., including solubility limitations), as indicated by the dotted lines in Fig. 9b, and compared to predicted κ applying a pure MNC κ of 0.16 (i.e., pure MNC κ in the absence of solubility limitations calculated from Eq. 6), as indicated by the dashed lines in

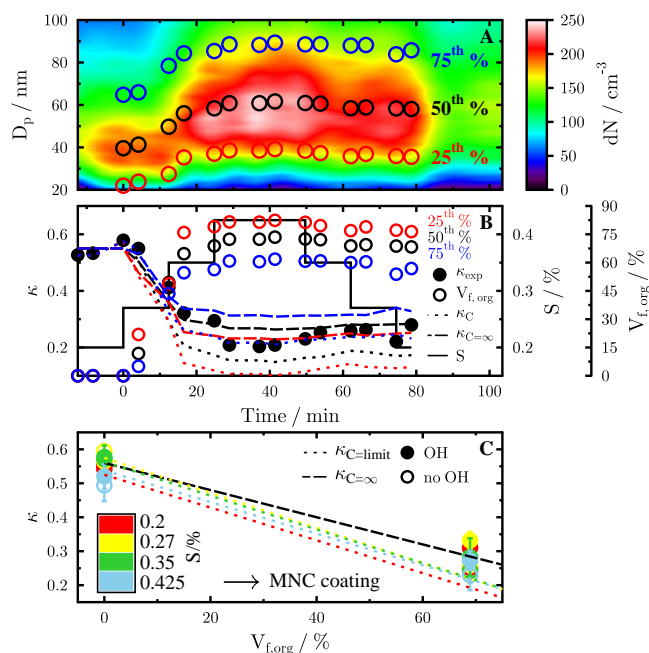


Figure 9. CCN activity of MNC-coated KS particles before and after exposure to OH. Panel (a) shows a color map of the number-weighted particle size distribution (dN) of KS and MNC-coated KS particles plotted as a function of MNC coating before exposure to OH. The open circles in panel (a) refer to the measured percentiles of the total particle population (25th: red; 50th: black; 75th: blue). Panel (b) displays the change in particle hygroscopicity (filled circles) and MNC volume fraction ($V_{f,org}$, open circles) with time as a function of S given as a black solid line corresponding to the data presented in panel (a). The dotted lines show the predicted κ using the volume mixing rule corresponding to the $V_{f,org}$ at a given time and based on the experimentally derived κ for KS and MNC given in Table 1 as a function of S . The dashed lines represent the predicted κ using the volume mixing rule corresponding to the $V_{f,org}$ at a given time and assuming the CCN activity of MNC is not limited by its solubility (i.e., MNC $\kappa = 0.16$ calculated from Eq. 6). Panel (c) displays the change in κ for the MNC-coated KS particles as a function of $V_{f,org}$, OH exposure, and S . OH unexposed particles are plotted as open circles. Filled circles correspond to particles exposed to OH at 3.3×10^{11} molecule cm^{-3} s. The error bars represent 1σ from the mean in κ . The colored dotted lines show predicted κ as a function of $V_{f,org}$ at different S using the volume mixing rule assuming the CCN activity of MNC is limited by its solubility. The black dashed line shows the predicted κ using the volume mixing rule assuming the CCN activity of MNC is not limited by its solubility.

Fig. 9b. The predicted κ with increasing $V_{f,org}$ generally captures the trend in experimentally derived κ with increasing $V_{f,org}$; however, similarly to the atomized MNC : KS binary-component particles, assuming MNC CCN activity is limited by its solubility, the volume mixing rule underpredicts derived κ . When applying a pure MNC $\kappa = 0.16$ in the absence of solubility limitations, the volume mixing rule is in slightly better agreement with the derived κ values. However,

there are notable deviations between derived κ and predicted κ in both cases, which depend on S . For example, in Fig. 9b, the predicted κ including MNC solubility limitations (dotted line) is in better agreement with the derived κ at $S = 0.425\%$ than at lower S . At higher S , the particles that activate first are smaller in diameter than the particles that activate first at lower S . Assuming differently sized KS particles were exposed to an equal quantity of gas-phase MNC, the larger particles, having relatively larger surface areas than the smaller KS particles, would acquire a thinner organic coating, and thus relatively smaller $V_{f,org}$. As a result, the particles that activate at $S = 0.425\%$ possess a larger $V_{f,org}$ compared to the particles that activate at, e.g., $S = 0.2\%$. This corresponds to a decrease in derived κ at $S = 0.425\%$ (i.e., better agreement with predicted κ including MNC solubility limitations) relative to other S as indicated in Fig. 9b. The generally better agreement in the predicted κ excluding MNC solubility limitations with the experimentally derived κ indicates that MNC is sufficiently water-soluble to not deactivate KS, in contrast to the particle systems studied by Abbatt et al. (2005). One possible explanation for the higher than expected κ when KS is coated with MNC is that the particle-phase diffusivity is sufficiently high to allow water molecules to penetrate the KS core (Koop et al., 2011).

The effects of OH exposure on the CCN activity of MNC-coated KS particles as a function of $V_{f,org}$ are given in Fig. 9c. κ is plotted as a function of MNC $V_{f,org}$. The κ values resulting from an OH exposure of 3.3×10^{11} molecule cm^{-3} s are given by the filled circles, whereby the different colors represent the applied S during the experiment. Open circles correspond to κ in the absence of OH. At $V_{f,org} = 0\%$, κ is ~ 0.55 and independent of OH exposure. κ decreases when $V_{f,org} \approx 70\%$, but undergoes a slight enhancement following OH exposure. The dotted lines indicate the modeled change in κ as a function of $V_{f,org}$ applying the volume mixing rule and applying the experimentally derived κ for MNC and KS at a given S (i.e., including MNC solubility limitations). Similar to the atomized 1 : 1 MNC : KS binary-component particles, modeled κ as a function of $V_{f,org}$ underpredicts the experimentally derived OH-unexposed κ , even after accounting for the enhancements in pure-component MNC κ due to the high OH exposure. This suggests that in the presence of KS at this $V_{f,org} \approx 70\%$, MNC may not be limited by its solubility, similar to the atomized 1 : 1 mass ratio MNC : KS binary-component particles, and that OH exposure can have very little impact on the CCN activity of sparingly soluble organics coated on water-soluble compounds. However, the dashed black line shows the modeled κ as a function of $V_{f,org}$ applying the volume mixing rule and assuming MNC is not limited by its solubility, i.e., MNC $\kappa = 0.16$, which slightly overpredicts the derived κ , but is in better agreement with the trend in experimentally derived κ for the OH-exposed particles (filled circles, Fig. 9c). A reasonable explanation for this is that $V_{f,org} \approx 70\%$ is sufficiently large such that MNC solubility limitations on the CCN activity of MNC-coated KS parti-

cles are partially exhibited. While OH exposure has a significant impact on the CCN activity of pure MNC, its impact on the CCN activity of MNC-coated KS particles is significantly less. The higher water solubility of KS appears to govern hygroscopic growth, similar to the atomized MNC : KS binary-component particles. This suggests that the water solubility of the more soluble component of mixed-component aerosol particles can be more important for CCN activation than the actual mixing state of the particle.

4 Conclusions

To our knowledge, there are no studies that have explicitly investigated the influence of OH-initiated oxidative aging on the hygroscopicity of organic and mixed organic–inorganic BBA particles. Biomass burning can greatly influence cloud formation and microphysical properties by increasing the available CCN in the atmosphere (Andreae et al., 2004). However, the efficiency at which aerosol particles act as CCN depends on their water solubility, hygroscopicity, and size, which can be altered by multiphase chemical reactions with gas-phase oxidants. While it is recognized that a significant fraction of BBA is comprised of organic material (Reid et al., 2005), most of which is water-soluble (Dusek et al., 2011; Graham et al., 2002), water uptake can be sensitive to the inorganic mass fraction (Semeniuk et al., 2007; Ruehl et al., 2012). In this study we investigated how sensitive the CCN activity of single-component and mixed water-soluble/water-insoluble compounds associated with BBA are to OH oxidation. The important findings relevant to the atmosphere include that (i) the hygroscopicity of water-soluble organic compounds is unaffected by chemical aging, (ii) the hygroscopicity of single-component water-insoluble organic compounds is affected by chemical aging as anticipated from previous studies (George et al., 2009; Lambe et al., 2011; Wong et al., 2011; Broekhuizen et al., 2004; Shilling et al., 2007; Petters et al., 2006), and (iii) if considering mixtures of water-soluble and insoluble materials, the effects of chemical aging by OH are more complicated, and single-component-derived κ and changes to κ as a function of OH exposure do not translate directly to mixtures.

WSOC constitutes a significant fraction of biomass burning OA (Graham et al., 2002; Reid et al., 2005; Saarikoski et al., 2007; Saarnio et al., 2010; Dusek et al., 2011) and atmospheric OA in general (Saxena and Hildemann, 1996; Timonen et al., 2013). Water-soluble OAs are effective CCN because they enhance the solute term in the Köhler equation. Chemical aging is known to promote the solubility of initially insoluble and sparingly soluble OA by yielding more water-soluble and multifunctional reaction products (George et al., 2009; Petters et al., 2006; Decesari et al., 2002). The question of atmospheric relevance depends on the concentration or potency of a particular molecule in the atmosphere. MNC, while contributing little to the mass fraction of BBA

particles, is toxic to forests (Harrison et al., 2005) and recognized as an important biomass burning SOA molecular marker (Iinuma et al., 2010). An OH exposure equivalent to only a few days of atmospheric exposure leads to an order of magnitude enhancement in MNC hygroscopicity. This implies that aged MNC is more susceptible to wet depositional losses over atmospherically relevant particle transport timescales, e.g., through cloud formation, compared to fresh MNC. Calculations from Petters et al. (2006) indicate that substantial wet depositional losses can occur when $\kappa > 0.01$. The question of the utility of MNC as a molecular marker for source apportionment is raised since molecular markers are assumed to be inert over the course of its lifetime in the atmosphere. Clearly, OH oxidation of MNC influences its chemical composition, but in doing so also decreases its atmospheric lifetime by enhancing its CCN activity. However, our results strongly suggest that if the OA is WSOC-dominated, e.g., by LEV, the reaction products likely have similar CCN activity to the parent WSOC, and thus particle oxidation plays a very minor role in enhancing the CCN activity of WSOC. Indeed, only a minor enhancement in the hygroscopicity of BBA, produced from controlled wood burning, was observed after several hours of photo-oxidation, likely a result of significant BBA WSOC content (Martin et al., 2013).

Much less is known of the effects of chemical aging on the CCN activity of internally mixed water-soluble and insoluble organic–inorganic particles. While oxidative aging can enhance the hygroscopicity of single-component particles with initially low water solubility, atmospheric aerosol particles are not often pure and consist of both organic and inorganic compounds (Laskin et al., 2012; Knopf et al., 2014; Murphy and Thomson, 1997; Murphy et al., 2006; Middlebrook et al., 1998). Organic compounds alone can influence the hygroscopicity of inorganic aerosol particles (Marcolli et al., 2004; Choi and Chan, 2002; Svenningsson et al., 2006; Wang et al., 2008) and moderate amounts of water-soluble inorganics can render low-solubility organics infinitely water-soluble (Bilde and Svenningsson, 2004; Abbatt et al., 2005; Shantz et al., 2008; Petters and Kreidenweis, 2008). When mixed with LEV or KS (or both) in significant mass fractions, the effects of OH oxidative aging on the hygroscopicity of single-component MNC are not revealed in the derived κ for the binary- or ternary-component particles. Furthermore, a thick coating of MNC on KS particles had similar impacts on the CCN activity behavior with increasing OH exposure as the atomized binary-component MNC : KS particles. The water-soluble fraction (i.e., KS) was sufficiently large that MNC became infinitely soluble. Our results indicate that it is the fraction of the water-soluble component of internally mixed water-soluble and insoluble organic–inorganic particles that dictates whether chemical aging will enhance the particles' CCN activity. Chemical aging has no major impact on the CCN activity of the mixed water-soluble and sparingly soluble BBA compounds studied here, beyond the point that the less water-soluble component becomes infinitely soluble.

Below this point, chemical aging can influence the CCN activity of the mixed particle. However, we caution against extrapolating general atmospheric conclusions given the limited number of compounds and mixtures studied here and suggest that similar work in the future also consider more complex, atmospherically relevant particle systems.

The Supplement related to this article is available online at doi:10.5194/acp-15-10183-2015-supplement.

Acknowledgements. J. H. Slade and D. A. Knopf acknowledge support from the National Science Foundation grants OCE-1336724 and AGS-0846255. J. Wang and R. Thalman acknowledge support from the US Department of Energy's Atmospheric System Research Program (Office of Science, OBER) under contract DE-AC02098CH10886.

Edited by: D. Topping

References

- Abbatt, J. P. D., Broekhuizen, K., and Kumal, P. P.: Cloud condensation nucleus activity of internally mixed ammonium sulfate/organic acid aerosol particles, *Atmos. Environ.*, 39, 4767–4778, doi:10.1016/j.atmosenv.2005.04.029, 2005.
- Abbatt, J. P. D., Lee, A. K. Y., and Thornton, J. A.: Quantifying trace gas uptake to tropospheric aerosol: recent advances and remaining challenges, *Chem. Soc. Rev.*, 41, 6555–6581, doi:10.1039/c2cs35052a, 2012.
- Anbar, M., Meyerstein, D., and Neta, P.: The reactivity of aromatic compounds toward hydroxyl radicals, *J. Phys. Chem.*, 70, 2660–2662, doi:10.1021/j100880a034, 1966.
- Andreae, M. O. and Rosenfeld, D.: Aerosol–cloud–precipitation interactions. Part 1. The nature and sources of cloud-active aerosols, *Earth-Sci. Rev.*, 89, 13–41, doi:10.1016/j.earscirev.2008.03.001, 2008.
- Andreae, M. O., Rosenfeld, D., Artaxo, P., Costa, A. A., Frank, G. P., Longo, K. M., and Silva-Dias, M. A. F.: Smoking rain clouds over the Amazon, *Science*, 303, 1337–1342, doi:10.1126/science.1092779, 2004.
- Arangio, A., Slade, J. H., Berkemeier, T., Pöschl, U., Knopf, D. A., and Shiraiwa, M.: Multiphase chemical kinetics of OH radical uptake by molecular organic markers of biomass burning aerosols: humidity and temperature dependence, surface reaction and bulk diffusion, *J. Phys. Chem. A.*, 119, 4533–4544, doi:10.1021/jp510489z, 2015.
- Bai, J., Sun, X., Zhang, C., Xu, Y., and Qi, C.: The OH-initiated atmospheric reaction mechanism and kinetics for levoglucosan emitted in biomass burning, *Chemosphere*, 93, 2004–2010, doi:10.1016/j.chemosphere.2013.07.021, 2013.
- Baustian, K. J., Cziczo, D. J., Wise, M. E., Pratt, K. A., Kulkarni, G., Hallar, A. G., and Tolbert, M. A.: Importance of aerosol composition, mixing state, and morphology for heterogeneous ice nucleation: a combined field and laboratory approach, *J. Geophys. Res.-Atmos.*, 117, D06217, doi:10.1029/2011JD016784, 2012.

- Bilde, M. and Svenningsson, B.: CCN activation of slightly soluble organics: the importance of small amounts of inorganic salt and particle phase, *Tellus B*, 56, 128–134, doi:10.1111/j.1600-0889.2004.00090.x, 2004.
- Bond, T., Streets, D., Yarber, K., Nelson, S., Woo, J.-H., and Klimont, Z.: A technology-based global inventory of black and organic carbon emissions from combustion, *J. Geophys. Res.*, 109, D14203, doi:10.1029/2003JD003697, 2004.
- Broekhuizen, K. E., Thornberry, T., Kumar, P. P., and Abbatt, J. P. D.: Formation of cloud condensation nuclei by oxidative processing: unsaturated fatty acids, *J. Geophys. Res.*, 109, S524–S537, doi:10.1029/2004JD005298, 2004.
- Brooks, S. D., Suter, K., and Olivarez, L.: Effects of chemical aging on the ice nucleation activity of soot and polycyclic aromatic hydrocarbon aerosols, *J. Phys. Chem. A*, 118, 10036–10047, doi:10.1021/jp508809y, 2014.
- Carrico, C. M., Petters, M. D., Kreidenweis, S. M., Sullivan, A. P., McMeeking, G. R., Levin, E. J. T., Engling, G., Malm, W. C., and Collett Jr., J. L.: Water uptake and chemical composition of fresh aerosols generated in open burning of biomass, *Atmos. Chem. Phys.*, 10, 5165–5178, doi:10.5194/acp-10-5165-2010, 2010.
- Chan, M. N., Choi, M. Y., Ng, N. L., and Chan, C. K.: Hygroscopicity of water-soluble organic compounds in atmospheric aerosols: amino acids and biomass burning derived organic species, *Environ. Sci. Technol.*, 39, 1555–1562, doi:10.1021/es049584i, 2005.
- Chen, L., Moosmuller, H., Arnott, W., Chow, J., Watson, J., Susott, R., Babbitt, R., Wold, C., Lincoln, E., Hao, W., Moosmuller, H., Arnott, W. P., Chow, J. C., Watson, J. G., Susott, R. A., Babbitt, R. E., Wold, C. E., Lincoln, E. N., and Hao, W. M.: Emissions from laboratory combustion of wildland fuels: emission factors and source profiles, *Environ. Sci. Technol.*, 41, 4317–4325, doi:10.1021/es062364i, 2007.
- Choi, M. Y. and Chan, C. K.: The effects of organic species on the hygroscopic behaviors of inorganic aerosols, *Environ. Sci. Technol.*, 36, 2422–2428, doi:10.1021/es0113293, 2002.
- Claeys, M., Vermeylen, R., Yasmeeen, F., Gómez-González, Y., Chi, X., Maenhaut, W., Mészáros, T., and Salma, I.: Chemical characterisation of humic-like substances from urban, rural and tropical biomass burning environments using liquid chromatography with UV/vis photodiode array detection and electrospray ionisation mass spectrometry, *Environ. Chem.*, 9, 273–284, doi:10.1071/EN11163, 2012.
- Collins, D. R., Flagan, R. C., and Seinfeld, J. H.: Improved inversion of scanning DMA data, *Aerosol Sci. Tech.*, 36, 1–9, doi:10.1080/027868202753339032, 2002.
- Cosman, L. M., Knopf, D. A., and Bertram, A. K.: N₂O₅ reactive uptake on aqueous sulfuric acid solutions coated with branched and straight-chain insoluble organic surfactants, *J. Phys. Chem. A*, 112, 2386–2396, doi:10.1021/jp710685r, 2008.
- Cruz, C. N. and Pandis, S. N.: The effect of organic coatings on the cloud condensation nuclei activation of inorganic atmospheric aerosol, *J. Geophys. Res.-Atmos.*, 103, 13111–13123, doi:10.1029/98JD00979, 1998.
- Decesari, S., Facchini, M. C., Matta, E., Mircea, M., Fuzzi, S., Chughtai, A. R., and Smith, D. M.: Water soluble organic compounds formed by oxidation of soot, *Atmos. Environ.*, 36, 1827–1832, doi:10.1016/S1352-2310(02)00141-3, 2002.
- Di Paola, A., Augugliaro, V., Palmisano, L., Pantaleo, G., and Savinov, E.: Heterogeneous photocatalytic degradation of nitrophenols, *J. Photoch. Photobio. A*, 155, 207–214, doi:10.1016/S1010-6030(02)00390-8, 2003.
- Dusek, U., Covert, D. S., Wiedensohler, A., Neususs, C., Weise, D., and Cantrell, W.: Cloud condensation nuclei spectra derived from size distributions and hygroscopic properties of the aerosol in coastal south-west Portugal during ACE-2, *Tellus B*, 55, 35–53, doi:10.1034/j.1600-0889.2003.00041.x, 2003.
- Dusek, U., Frank, G. P., Hildebrandt, L., Curtius, J., Schneider, J., Walter, S., Chand, D., Drewnick, F., Hings, S., Jung, D., Borrmann, S., and Andreae, M. O.: Size matters more than chemistry for cloud-nucleating ability of aerosol particles, *Science*, 312, 1375–1378, doi:10.1126/science.1125261, 2006.
- Dusek, U., Frank, G. P., Massling, A., Zeromskiene, K., Iinuma, Y., Schmid, O., Helas, G., Hennig, T., Wiedensohler, A., and Andreae, M. O.: Water uptake by biomass burning aerosol at sub- and supersaturated conditions: closure studies and implications for the role of organics, *Atmos. Chem. Phys.*, 11, 9519–9532, doi:10.5194/acp-11-9519-2011, 2011.
- Ellison, G. B., Tuck, A. F., and Vaida, V.: Atmospheric processing of organic aerosols, *J. Geophys. Res.-Atmos.*, 104, 11633–11641, doi:10.1029/1999JD900073, 1999.
- EPI (Estimation Program Interface): US EPA. Estimation Programs Interface Suite™ for Microsoft®, v 4.11. United States Environmental Protection Agency, Washington, DC, USA, 2015.
- Ervens, B., Feingold, G., and Kreidenweis, S. M.: Influence of water-soluble organic carbon on cloud drop number concentration, *J. Geophys. Res.-Atmos.*, 110, D18211, doi:10.1029/2004JD005634, 2005.
- Friedman, B., Kulkarni, G., Beránek, J., Zelenyuk, A., Thornton, J. A., and Cziczo, D. J.: Ice nucleation and droplet formation by bare and coated soot particles, *J. Geophys. Res.*, 116, D17203, doi:10.1029/2011JD015999, 2011.
- Fuchs, N. A. and Sutugin, A. G.: Highly Dispersed Aerosols, 2nd edn., Ann Arbor Sci., Ann Arbor, MI, USA, 1970.
- Garland, R. M., Wise, M. E., Beaver, M. R., DeWitt, H. L., Aiken, A. C., Jimenez, J. L., and Tolbert, M. A.: Impact of palmitic acid coating on the water uptake and loss of ammonium sulfate particles, *Atmos. Chem. Phys.*, 5, 1951–1961, doi:10.5194/acp-5-1951-2005, 2005.
- Gasparini, R., Li, R. J., Collins, D. R., Ferrare, R. A., and Brackett, V. G.: Application of aerosol hygroscopicity measured at the Atmospheric Radiation Measurement Program's Southern Great Plains site to examine composition and evolution, *J. Geophys. Res.-Atmos.*, 111, D05S12, doi:10.1029/2004JD005448, 2006.
- George, I. and Abbatt, J.: Heterogeneous oxidation of atmospheric aerosol particles by gas-phase radicals, *Nat. Chem.*, 2, 713–722, doi:10.1038/nchem.806, 2010.
- George, I. J., Chang, R. Y.-W., Danov, V., Vlasenko, A., and Abbatt, J. P. D.: Modification of cloud condensation nucleus activity of organic aerosols by hydroxyl radical heterogeneous oxidation, *Atmos. Environ.*, 43, 5038–5045, doi:10.1016/j.atmosenv.2009.06.043, 2009.
- Gierlus, K. M., Laskina, O., Abernathy, T. L., and Grassian, V. H.: Laboratory study of the effect of oxalic acid on the cloud condensation nuclei activity of mineral dust aerosol, *Atmos. Environ.*, 46, 125–130, doi:10.1016/j.atmosenv.2011.10.027, 2012.
- Giordano, M., Espinoza, C., and Asa-Awuku, A.: Experimentally measured morphology of biomass burning aerosol and its im-

- pacts on CCN ability, *Atmos. Chem. Phys.*, 15, 1807–1821, doi:10.5194/acp-15-1807-2015, 2015.
- Graham, B., Mayol-Bracero, O. L., Guyon, P., Roberts, G. C., Decesari, S., Facchini, M. C., Artaxo, P., Maenhaut, W., Koll, P., and Andreae, M. O.: Water-soluble organic compounds in biomass burning aerosols over Amazonia – 1. Characterization by NMR and GC-MS, *J. Geophys. Res.-Atmos.*, 107, LBA 14-1–LBA 14-16, doi:10.1029/2001JD000336, 2002.
- Grieshop, A. P., Logue, J. M., Donahue, N. M., and Robinson, A. L.: Laboratory investigation of photochemical oxidation of organic aerosol from wood fires 1: measurement and simulation of organic aerosol evolution, *Atmos. Chem. Phys.*, 9, 1263–1277, doi:10.5194/acp-9-1263-2009, 2009.
- Gunthe, S. S., King, S. M., Rose, D., Chen, Q., Roldin, P., Farmer, D. K., Jimenez, J. L., Artaxo, P., Andreae, M. O., Martin, S. T., and Pöschl, U.: Cloud condensation nuclei in pristine tropical rainforest air of Amazonia: size-resolved measurements and modeling of atmospheric aerosol composition and CCN activity, *Atmos. Chem. Phys.*, 9, 7551–7575, doi:10.5194/acp-9-7551-2009, 2009.
- Hallquist, M., Wenger, J. C., Baltensperger, U., Rudich, Y., Simpson, D., Claeys, M., Dommen, J., Donahue, N. M., George, C., Goldstein, A. H., Hamilton, J. F., Herrmann, H., Hoffmann, T., Iinuma, Y., Jang, M., Jenkin, M. E., Jimenez, J. L., Kiendler-Scharr, A., Maenhaut, W., McFiggans, G., Mentel, Th. F., Monod, A., Prévôt, A. S. H., Seinfeld, J. H., Surratt, J. D., Szmigielski, R., and Wildt, J.: The formation, properties and impact of secondary organic aerosol: current and emerging issues, *Atmos. Chem. Phys.*, 9, 5155–5236, doi:10.5194/acp-9-5155-2009, 2009.
- Harmon, C. W., Ruehl, C. R., Cappa, C. D., and Wilson, K. R.: A statistical description of the evolution of cloud condensation nuclei activity during the heterogeneous oxidation of squalane and bis(2-ethylhexyl) sebacate aerosol by hydroxyl radicals, *Phys. Chem. Chem. Phys.*, 15, 9679–9693, doi:10.1039/C3CP50347J, 2013.
- Harrison, M. A. J., Barra, S., Borghesi, D., Vione, D., Arsene, C., and Olariu, R. I.: Nitrated phenols in the atmosphere: a review, *Atmos. Environ.*, 39, 231–248, doi:10.1016/j.atmosenv.2004.09.044, 2005.
- Hays, M. D., Fine, P. M., Geron, C. D., Kleeman, M. J., and Gullett, B. K.: Open burning of agricultural biomass: physical and chemical properties of particle-phase emissions, *Atmos. Environ.*, 39, 6747–6764, doi:10.1016/j.atmosenv.2005.07.072, 2005.
- Hoffmann, D., Tilgner, A., Iinuma, Y., and Herrmann, H.: Atmospheric stability of levoglucosan: a detailed laboratory and modeling study, *Environ. Sci. Technol.*, 44, 694–699, doi:10.1021/es902476f, 2010.
- Iinuma, Y., Brüggemann, E., Gnauk, T., Müller, K., Andreae, M., Helas, G., Parmar, R., and Herrmann, H.: Source characterization of biomass burning particles: the combustion of selected European conifers, African hardwood, savanna grass, and German and Indonesian peat, *J. Geophys. Res.*, 112, D08209, doi:10.1029/2006JD007120, 2007.
- Iinuma, Y., Boge, O., Grafe, R., and Herrmann, H.: Methyl-nitrocatechols: atmospheric tracer compounds for biomass burning secondary organic aerosols, *Environ. Sci. Technol.*, 44, 8453–8459, doi:10.1021/es102938a, 2010.
- Jathar, S. H., Gordon, T. D., Hennigan, C. J., Pye, H. O. T., Pouliot, G., Adams, P. J., Donahue, N. M., and Robinson, A. L.: Unspeciated organic emissions from combustion sources and their influence on the secondary organic aerosol budget in the United States, *P. Natl. Acad. Sci. USA*, 111, 10473–10478, doi:10.1073/pnas.1323740111, 2014.
- Kaiser, J. C., Riemer, N., and Knopf, D. A.: Detailed heterogeneous oxidation of soot surfaces in a particle-resolved aerosol model, *Atmos. Chem. Phys.*, 11, 4505–4520, doi:10.5194/acp-11-4505-2011, 2011.
- Katrib, Y., Martin, S. T., Hung, H. M., Rudich, Y., Zhang, H. Z., Slowik, J. G., Davidovits, P., Jayne, J. T., and Worsnop, D. R.: Products and mechanisms of ozone reactions with oleic acid for aerosol particles having core-shell morphologies, *J. Phys. Chem. A*, 108, 6686–6695, doi:10.1021/jp049759d, 2004.
- Kessler, S. H., Smith, J. D., Che, D. L., Worsnop, D. R., Wilson, K. R., and Kroll, J. H.: Chemical sinks of organic aerosol: kinetics and products of the heterogeneous oxidation of erythritol and levoglucosan, *Environ. Sci. Technol.*, 44, 7005–7010, doi:10.1021/es101465m, 2010.
- Knopf, D. A., Cosman, L. M., Mousavi, P., Mokamati, S., and Bertram, A. K.: A novel flow reactor for studying reactions on liquid surfaces coated by organic monolayers: methods, validation, and initial results, *J. Phys. Chem. A*, 111, 11021–11032, 2007.
- Knopf, D. A., Forrester, S. M., and Slade, J. H.: Heterogeneous oxidation kinetics of organic biomass burning aerosol surrogates by O₃, NO₂, N₂O₅, and NO₃, *Phys. Chem. Chem. Phys.*, 13, 21050–21062, doi:10.1039/c1cp22478f, 2011.
- Knopf, D. A., Alpert, P. A., Wang, B., O'Brien, E., Kelly, S. T., Laskin, A., Gilles, K., and Moffet, R. C.: Microspectroscopic imaging and characterization of individually identified ice nucleating particles from a case field study, *J. Geophys. Res.*, 119, 10365–10381, doi:10.1002/2014JD021866, 2014.
- Koop, T., Bookhold, J., Shiraiwa, M., and Pöschl, U.: Glass transition and phase state of organic compounds: dependency on molecular properties and implications for secondary organic aerosols in the atmosphere, *Phys. Chem. Chem. Phys.*, 13, 19238–19255, doi:10.1039/C1CP22617G, 2011.
- Lambe, A. T., Onasch, T. B., Massoli, P., Croasdale, D. R., Wright, J. P., Ahern, A. T., Williams, L. R., Worsnop, D. R., Brune, W. H., and Davidovits, P.: Laboratory studies of the chemical composition and cloud condensation nuclei (CCN) activity of secondary organic aerosol (SOA) and oxidized primary organic aerosol (OPOA), *Atmos. Chem. Phys.*, 11, 8913–8928, doi:10.5194/acp-11-8913-2011, 2011.
- Lance, S., Medina, J., Smith, J. N., and Nenes, A.: Mapping the operation of the DMT Continuous Flow CCN counter, *Aerosol Sci. Tech.*, 40, 242–254, doi:10.1080/02786820500543290, 2006.
- Laskin, A., Moffet, R. C., Gilles, M. K., Fast, J. D., Zaveri, R. A., Wang, B., Nigge, P., and Shutthanandan, J.: Tropospheric chemistry of internally mixed sea salt and organic particles: surprising reactivity of NaCl with weak organic acids, *J. Geophys. Res.*, 117, D15302, doi:10.1029/2012JD017743, 2012.
- Low, R. D. H.: A comprehensive report on nineteen condensation nuclei. Part 1. Equilibrium growth and physical properties, Res. Rep. Ad 691700, ECO-5249, Atmospheric Sciences Lab, White Sands Missile Range, NM, US Army Electronics Command (ECO), Fort Monmouth, New Jersey, USA, 1969.

- Marcolli, C., Luo, B. P., and Peter, T.: Mixing of the organic aerosol fractions: liquids as the thermodynamically stable phases, *J. Phys. Chem. A*, 108, 2216–2224, doi:10.1021/jp036080l, 2004.
- Martin, M., Tritscher, T., Jurányi, Z., Heringa, M. F., Sierau, B., Weingartner, E., Chirico, R., Gysel, M., Prévôt, A. S. H., Baltensperger, U., and Lohmann, U.: Hygroscopic properties of fresh and aged wood burning particles, *J. Aerosol. Sci.*, 56, 15–29, doi:10.1016/j.jaerosci.2012.08.006, 2013.
- Massoli, P., Lambe, A. T., Ahern, A. T., Williams, L. R., Ehn, M., Mikkilä, J., Canagaratna, M. R., Brune, W. H., Onasch, T. B., Jayne, J. T., Petäjä, T., Kulmala, M., Laaksonen, A., Kolb, C. E., Davidovits, P., and Worsnop, D. R.: Relationship between aerosol oxidation level and hygroscopic properties of laboratory generated secondary organic aerosol (SOA) particles, *Geophys. Res. Lett.*, 37, L24801, doi:10.1029/2010GL045258, 2010.
- Mei, F., Hayes, P. L., Ortega, A., Taylor, J. W., Allan, J. D., Gilman, J., Kuster, W., de Gouw, J., Jimenez, J. L., and Wang, J.: Droplet activation properties of organic aerosols observed at an urban site during CalNex-LA, *J. Geophys. Res.-Atmos.*, 118, 2903–2917, doi:10.1002/jgrd.50285, 2013a.
- Mei, F., Setyan, A., Zhang, Q., and Wang, J.: CCN activity of organic aerosols observed downwind of urban emissions during CARES, *Atmos. Chem. Phys.*, 13, 12155–12169, doi:10.5194/acp-13-12155-2013, 2013b.
- Middlebrook, A. M., Murphy, D. M., and Thomson, D. S.: Observations of organic material in individual marine particles at Cape Grim during the First Aerosol Characterization Experiment (ACE 1), *J. Geophys. Res.*, 103, 16475–16483, doi:10.1029/97JD03719, 1998.
- Mikhailov, E., Vlasenko, S., Martin, S. T., Koop, T., and Pöschl, U.: Amorphous and crystalline aerosol particles interacting with water vapor: conceptual framework and experimental evidence for restructuring, phase transitions and kinetic limitations, *Atmos. Chem. Phys.*, 9, 9491–9522, doi:10.5194/acp-9-9491-2009, 2009.
- Möhler, O., Benz, S., Saathoff, H., Schnaiter, M., Wagner, R., Schneider, J., Walter, S., Ebert, V., and Wagner, S.: The effect of organic coating on the heterogeneous ice nucleation efficiency of mineral dust aerosols, *Environ. Res. Lett.*, 3, 025007, doi:10.1088/1748-9326/3/2/025007, 2008.
- Monks, P. S., Granier, C., Fuzzi, S., Stohl, A., Williams, M. L., Akiyama, H., Amann, M., Baklanov, A., Baltensperger, U., Bey, I., Blake, N., Blake, R. S., Carslaw, K., Cooper, O. R., Dentener, F., Fowler, D., Fragkou, E., Frost, G. J., Generoso, S., Ginoux, P., Grewe, V., Guenther, A., Hansson, H. C., Henne, S., Hjorth, J., Hofzumahaus, A., Huntrieser, H., Isaksen, I. S. A., Jenkin, M. E., Kaiser, J., Kanakidou, M., Klimont, Z., Kulmala, M., Laj, P., Lawrence, M. G., Lee, J. D., Liousse, C., Maione, M., McFiggans, G., Metzger, A., Mieville, A., Mousiopoulos, N., Orlando, J. J., O'Dowd, C. D., Palmer, P. I., Parrish, D. D., Petzold, A., Platt, U., Pöschl, U., Prévôt, A. S. H., Reeves, C. E., Reimann, S., Rudich, Y., Sellegri, K., Steinbrecher, R., Simpson, D., ten Brink, H., Theloke, J., van der Werf, G. R., Vautard, R., Vestreng, V., Vlachokostas, C., and von Glasow, R.: Atmospheric composition change – global and regional air quality, *Atmos. Environ.*, 43, 5268–5350, doi:10.1016/j.atmosenv.2009.08.021, 2009.
- Murphy, D. M. and Thomson, D. S.: Chemical composition of single aerosol particles at Idaho Hill: negative ion measurements, *J. Geophys. Res.-Atmos.*, 102, 6353–6368, doi:10.1029/96JD00859, 1997.
- Murphy, D. M., Cziczo, D. J., Froyd, K. D., Hudson, P. K., Matthew, B. M., Middlebrook, A. M., Peltier, R. E., Sullivan, A., Thomson, D. S., and Weber, R. J.: Single-particle mass spectrometry of tropospheric aerosol particles, *J. Geophys. Res.*, 111, D23S32, doi:10.1029/2006JD007340, 2006.
- Novakov, T. and Corrigan, C. E.: Cloud condensation nucleus activity of the organic component of biomass smoke particles, *Geophys. Res. Lett.*, 23, 2141–2144, doi:10.1029/96GL01971, 1996.
- Nozière, B., Baduel, C., and Jaffrezo, J.-L.: The dynamic surface tension of atmospheric aerosol surfactants reveals new aspects of cloud activation, *Nat. Comm.*, 5, 3335, doi:10.1038/ncomms4335, 2014.
- Park, S.-C., Burden, D. K., and Nathanson, G. M.: The inhibition of N₂O₅ hydrolysis in sulfuric acid by 1-butanol and 1-hexanol surfactant coatings, *J. Phys. Chem. A*, 111, 2921–2929, doi:10.1021/jp068228h, 2007.
- Petters, M. D. and Kreidenweis, S. M.: A single parameter representation of hygroscopic growth and cloud condensation nucleus activity, *Atmos. Chem. Phys.*, 7, 1961–1971, doi:10.5194/acp-7-1961-2007, 2007.
- Petters, M. D. and Kreidenweis, S. M.: A single parameter representation of hygroscopic growth and cloud condensation nucleus activity – Part 2: Including solubility, *Atmos. Chem. Phys.*, 8, 6273–6279, doi:10.5194/acp-8-6273-2008, 2008.
- Petters, M. D., Prenne, A. J., and Kreidenweis, S. M.: Chemical aging and the hydrophobic-to-hydrophilic conversion of carbonaceous aerosol, *Geophys. Res. Lett.*, 33, L24806, doi:10.1029/2006GL027249, 2006.
- Petters, M. D., Carrico, C. M., Kreidenweis, S. M., Prenni, A. J., DeMott, P. J., Collett Jr., J. L., and Moosmüller, H.: Cloud condensation nucleation activity of biomass burning aerosol, *J. Geophys. Res.*, 114, D22205, doi:10.1029/2009JD012353, 2009.
- Pöschl, U.: Atmospheric aerosols: composition, transformation, climate and health effects, *Angew. Chem. Int. Edit.*, 44, 7520–7540, doi:10.1002/anie.200501122, 2005.
- Pöschl, U.: Gas-particle interactions of tropospheric aerosols: kinetic and thermodynamic perspectives of multiphase chemical reactions, amorphous organic substances, and the activation of cloud condensation nuclei, *Atmos. Res.*, 101, 562–573, doi:10.1016/j.atmosres.2010.12.018, 2011.
- Pöschl, U., Letzel, T., Schauer, C., and Niessner, R.: Interaction of ozone and water vapor with spark discharge soot aerosol particles coated with benzo[a]pyrene: O₃ and H₂O adsorption, benzo[a]pyrene degradation, and atmospheric implications, *J. Phys. Chem. A*, 105, 4029–4041, doi:10.1021/jp004137n, 2001.
- Pósfai, M., Xu, H. F., Anderson, J. R., and Buseck, P. R.: Wet and dry sizes of atmospheric aerosol particles: an AFM-TFM study, *Geophys. Res. Lett.*, 25, 1907–1910, doi:10.1029/98GL01416, 1998.
- Pósfai, M., Simonics, R., Li, J., Hobbs, P. V., and Buseck, P. R.: Individual aerosol particles from biomass burning in southern Africa: 1. Compositions and size distributions of carbonaceous particles, *J. Geophys. Res.-Atmos.*, 108, 231–240, doi:10.1029/2002JD002291, 2003.
- Randerson, J. T., Chen, Y., van der Werf, G. R., Rogers, B. M., and Morton, D. C.: Global burned area and biomass burning emis-

- sions from small fires, *J. Geophys. Res.-Biogeo.*, 117, G04012, doi:10.1029/2012JG002128, 2012.
- Reid, J. S., Eck, T. F., Christopher, S. A., Koppmann, R., Dubovik, O., Eleuterio, D. P., Holben, B. N., Reid, E. A., and Zhang, J.: A review of biomass burning emissions part III: intensive optical properties of biomass burning particles, *Atmos. Chem. Phys.*, 5, 827–849, doi:10.5194/acp-5-827-2005, 2005.
- Renbaum, L. H. and Smith, G. D.: Artifacts in measuring aerosol uptake kinetics: the roles of time, concentration and adsorption, *Atmos. Chem. Phys.*, 11, 6881–6893, doi:10.5194/acp-11-6881-2011, 2011.
- Rissler, J., Vestin, A., Swietlicki, E., Fisch, G., Zhou, J., Artaxo, P., and Andreae, M. O.: Size distribution and hygroscopic properties of aerosol particles from dry-season biomass burning in Amazonia, *Atmos. Chem. Phys.*, 6, 471–491, doi:10.5194/acp-6-471-2006, 2006.
- Roberts, G., Artaxo, P., Zhou, J., Swietlicki, E., and Andreae, M. O.: Sensitivity of CCN spectra on chemical and physical properties of aerosol: a case study from the Amazon Basin, *J. Geophys. Res.*, 107, LBA 37-1–LBA 37-18, doi:10.1029/2001JD000583, 2002.
- Roberts, G. C. and Nenes, A.: A continuous-flow streamwise thermal-gradient CCN chamber for atmospheric measurements, *Aerosol Sci. Tech.*, 39, 206–221, doi:10.1080/027868290913988, 2005.
- Rose, D., Gunthe, S. S., Mikhailov, E., Frank, G. P., Dusek, U., Andreae, M. O., and Pöschl, U.: Calibration and measurement uncertainties of a continuous-flow cloud condensation nuclei counter (DMT-CCNC): CCN activation of ammonium sulfate and sodium chloride aerosol particles in theory and experiment, *Atmos. Chem. Phys.*, 8, 1153–1179, doi:10.5194/acp-8-1153-2008, 2008.
- Rose, D., Nowak, A., Achtert, P., Wiedensohler, A., Hu, M., Shao, M., Zhang, Y., Andreae, M. O., and Pöschl, U.: Cloud condensation nuclei in polluted air and biomass burning smoke near the mega-city Guangzhou, China – Part I: Size-resolved measurements and implications for the modeling of aerosol particle hygroscopicity and CCN activity, *Atmos. Chem. Phys.*, 10, 3365–3383, doi:10.5194/acp-10-3365-2010, 2010.
- Rudich, Y.: Laboratory perspectives on the chemical transformations of organic matter in atmospheric particles, *Chem. Rev.*, 103, 5097–5124, doi:10.1021/cr020508f, 2003.
- Rudich, Y., Donahue, N. M., and Mentel, T. F.: Aging of organic aerosol: bridging the gap between laboratory and field studies, *Annu. Rev. Phys. Chem.*, 58, 321–352, doi:10.1146/annurev.physchem.58.032806.104432, 2007.
- Ruehl, C. R., Chuang, P. Y., Nenes, A., Cappa, C. D., Kolesar, K. R., and Goldstein, A. H.: Strong evidence of surface tension reduction in microscopic aqueous droplets, *Geophys. Res. Lett.*, 39, L23801, doi:10.1029/2012GL053706, 2012.
- Russell, L. M., Maria, S. F., and Myneni, S. C. B.: Mapping organic coatings on atmospheric particles, *Geophys. Res. Lett.*, 29, 261–264, doi:10.1029/2002GL014874, 2002.
- Saarikoski, S., Sillanpää, M., Sofiev, M., Timonen, H., Saarnio, K., Teinela, K., Karppinen, A., Kukkonen, J., and Hillamo, R.: Chemical composition of aerosols during a major biomass burning episode over northern Europe in spring 2006: experimental and modelling assessments, *Atmos. Environ.*, 41, 3577–3589, doi:10.1016/j.atmosenv.2006.12.053, 2007.
- Saarnio, K., Aurela, M., Timonen, H., Saarikoski, S., Teinilä, K., Mäkelä, T., Sofiev, M., Koskinen, J., Aalto, P. P., Kulmala, M., Kukkonen, J., and Hillamo, R.: Chemical composition of fine particles in fresh smoke plumes from boreal wild-land fires in Europe, *Sci. Total Environ.*, 408, 2527–2542, doi:10.1016/j.scitotenv.2010.03.010, 2010.
- Saxena, P. and Hildemann, L. M.: Water-soluble organics in atmospheric particles: a critical review of the literature and application of thermodynamics to identify candidate compounds, *J. Atmos. Chem.*, 24, 57–109, doi:10.1007/BF00053823, 1996.
- Schauer, J. J., Kleeman, M. J., Cass, G. R., and Simoneit, B. R. T.: Measurement of emissions from air pollution sources. 3. C-1–C-29 organic compounds from fireplace combustion of wood, *Environ. Sci. Technol.*, 35, 1716–1728, doi:10.1021/es001331e, 2001.
- Schwier, A., Mitroo, D., and McNeill, V. F.: Surface tension depression by low-solubility organic material in aqueous aerosol mimics, *Atmos. Environ.*, 54, 490–495, doi:10.1016/j.atmosenv.2012.02.032, 2012.
- Semeniuk, T. A., Wise, M. E., Martin, S. T., Russell, L. M., and Buseck, P. R.: Hygroscopic behavior of aerosol particles from biomass fires using environmental transmission electron microscopy, *J. Atmos. Chem.*, 56, 259–273, doi:10.1007/s10874-006-9055-5, 2007.
- Shantz, N. C., Leitch, W. R., Phinney, L., Mozurkewich, M., and Toom-Sauntry, D.: The effect of organic compounds on the growth rate of cloud droplets in marine and forest settings, *Atmos. Chem. Phys.*, 8, 5869–5887, doi:10.5194/acp-8-5869-2008, 2008.
- Sheffield, A. E., Gordon, G. E., Currie, L. A., and Riederer, G. E.: Organic, elemental, and isotopic tracers of air-pollution sources in Albuquerque, NM, *Atmos. Environ.*, 28, 1371–1384, doi:10.1016/1352-2310(94)90200-3, 1994.
- Shilling, J. E., King, S. M., Mochida, M., Worsnop, D. R., and Martin, S. T.: Mass spectral evidence that small changes in composition caused by oxidative aging processes alter aerosol CCN properties, *J. Phys. Chem. A*, 111, 3358–3368, doi:10.1021/jp068822r, 2007.
- Simoneit, B. R. T.: A review of biomarker compounds as source indicators and tracers for air pollution, *Environ. Sci. Pollut. R.*, 6, 159–169, doi:10.1007/BF02987621, 1999.
- Slade, J. H. and Knopf, D. A.: Heterogeneous OH oxidation of biomass burning organic aerosol surrogate compounds: assessment of volatilisation products and the role of OH concentration on the reactive uptake kinetics, *Phys. Chem. Chem. Phys.*, 15, 5898–5915, doi:10.1039/c3cp44695f, 2013.
- Slade, J. H. and Knopf, D. A.: Multiphase OH oxidation kinetics of organic aerosol: the role of particle phase state and relative humidity, *Geophys. Res. Lett.*, 41, 5297–5306, doi:10.1002/2014GL060582, 2014.
- Springmann, M., Knopf, D. A., and Riemer, N.: Detailed heterogeneous chemistry in an urban plume box model: reversible co-adsorption of O₃, NO₂, and H₂O on soot coated with benzo[a]pyrene, *Atmos. Chem. Phys.*, 9, 7461–7479, doi:10.5194/acp-9-7461-2009, 2009.
- Stocker, T. F., Qin, D., Plattner, G. K., Tignor, M., Allen, S. K., Boschung, J., Nauels, A., Xia, Y., Bex, V., and Midgley, P. M.: *Climate Change 2013: the Physical Science Basis*, contribution of Working Group I to the Fifth Assessment Report of the Inter-

- governmental Panel on Climate Change, Cambridge University Press, Cambridge, UK, and New York, NY, USA, 2013.
- Suda, S. R., Petters, M. D., Yeh, G. K., Strollo, C., Matsunaga, A., Faulhaber, A., Ziemann, P. J., Prenni, A. J., Carrico, C. M., Sullivan, R. C., and Kreidenweis, S. M.: Influence of functional groups on organic aerosol cloud condensation nucleus activity, *Environ. Sci. Technol.*, 48, 10182–10190, doi:10.1021/es502147y, 2014.
- Svenningsson, B., Rissler, J., Swietlicki, E., Mircea, M., Bilde, M., Facchini, M. C., Decesari, S., Fuzzi, S., Zhou, J., Mønster, J., and Rosenørn, T.: Hygroscopic growth and critical supersaturations for mixed aerosol particles of inorganic and organic compounds of atmospheric relevance, *Atmos. Chem. Phys.*, 6, 1937–1952, doi:10.5194/acp-6-1937-2006, 2006.
- Timonen, H., Carbone, S., Aurela, M., Saarnio, K., Saarikoski, S., Ng, N. L., Canagaratna, M. R., Kulmala, M., Kerminen, V. M., Worsnop, D. R., and Hillamo, R.: Characteristics, sources and water-solubility of ambient submicron organic aerosol in springtime in Helsinki, Finland, *J. Aerosol Sci.*, 56, 61–77, doi:10.1016/j.jaerosci.2012.06.005, 2013.
- Tuckermann, R.: Surface tension of aqueous solutions of water-soluble organic and inorganic compounds, *Atmos. Environ.*, 41, 6265–6274, doi:10.1016/j.atmosenv.2007.03.051, 2007.
- Tuckermann, R. and Cammenga, H. K.: The surface tension of aqueous solutions of some atmospheric water-soluble organic compounds, *Atmos. Environ.*, 38, 6135–6138, doi:10.1016/j.atmosenv.2004.08.005, 2004.
- van der Werf, G. R., Randerson, J. T., Giglio, L., Collatz, G. J., Kasibhatla, P. S., and Arellano Jr., A. F.: Interannual variability in global biomass burning emissions from 1997 to 2004, *Atmos. Chem. Phys.*, 6, 3423–3441, doi:10.5194/acp-6-3423-2006, 2006.
- Wang, B. and Knopf, D. A.: Heterogeneous ice nucleation on particles composed of humic-like substances impacted by O₃, *J. Geophys. Res.*, 116, D03205, doi:10.1029/2010JD014964, 2011.
- Wang, B., Laskin, A., Roedel, T., Gilles, M. K., Moffet, R. C., Tivanski, A., and Knopf, D. A.: Heterogeneous ice nucleation and water uptake by field-collected atmospheric particles below 273 K, *J. Geophys. Res.*, 117, D00V19, doi:10.1029/2012JD017446, 2012.
- Wang, J., Lee, Y.-N., Daum, P. H., Jayne, J., and Alexander, M. L.: Effects of aerosol organics on cloud condensation nucleus (CCN) concentration and first indirect aerosol effect, *Atmos. Chem. Phys.*, 8, 6325–6339, doi:10.5194/acp-8-6325-2008, 2008.
- Wong, J. P. S., Lee, A. K. Y., Slowik, J. G., Cziczo, D. J., Leaitch, W. R., Macdonald, A., and Abbatt, J. P. D.: Oxidation of ambient biogenic secondary organic aerosol by hydroxyl radicals: effects on cloud condensation nuclei activity, *Geophys. Res. Lett.*, 38, L22805, doi:10.1029/2011GL049351, 2011.
- Zhang, Q., Jimenez, J. L., Canagaratna, M. R., Allan, J. D., Coe, H., Ulbrich, I., Alfarra, M. R., Takami, A., Middlebrook, A. M., Sun, Y. L., Dzepina, K., Dunlea, E., Docherty, K., DeCarlo, P. F., Salcedo, D., Onasch, T., Jayne, J. T., Miyoshi, T., Shimojo, A., Hatakeyama, S., Takegawa, N., Kondo, Y., Schneider, J., Dewnick, F., Borrmann, S., Weimer, S., Demerjian, K., Williams, P., Bower, K., Bahreini, R., Cottrell, L., Griffin, R. J., Rautiainen, J., Sun, J. Y., Zhang, Y. M., and Worsnop, D. R.: Ubiquity and dominance of oxygenated species in organic aerosols in anthropogenically-influenced Northern Hemisphere midlatitudes, *Geophys. Res. Lett.*, 34, L13801, doi:10.1029/2007GL029979, 2007.
- Zhao, R., Mungall, E. L., Lee, A. K. Y., Aljawhary, D., and Abbatt, J. P. D.: Aqueous-phase photooxidation of levoglucosan – a mechanistic study using aerosol time-of-flight chemical ionization mass spectrometry (Aerosol ToF-CIMS), *Atmos. Chem. Phys.*, 14, 9695–9706, doi:10.5194/acp-14-9695-2014, 2014.